Journal of the Mechanics and Physics of Solids 57 (2009) 1267–1292

Contents lists available at ScienceDirect

Journal of the Mechanics and Physics of Solids

journal homepage: www.elsevier.com/locate/jmps

On the origin of shear banding instability in metallic glasses

M.Q. Jiang, L.H. Dai *

State Key Laboratory of Nonlinear Mechanics, Institute of Mechanics, Chinese Academy of Sciences, Beijing 100190, PR China

ARTICLE INFO

Article history:
Received 20 October 2008
Received in revised form
13 April 2009
Accepted 21 April 2009

Keywords:
Metallic glasses
Free volume
Temperature increase
Shear-banding instability
Dilatation

ABSTRACT

To uncover the physical origin of shear-banding instability in metallic glass (MG), a theoretical description of thermo-mechanical deformation of MG undergoing one-dimensional simple shearing is presented. The coupled thermo-mechanical model takes into account the momentum balance, the energy balance and the dynamics of free volume. The interplay between free-volume production and temperature increase being two potential causes for shear-banding instability is examined on the basis of the homogeneous solution. It is found that the free-volume production facilitates the sudden increase in the temperature before instability and vice versa. A rigorous linear perturbation analysis is used to examine the inhomogeneous deformation, during which the onset criteria and the internal length and time scales for three types of instabilities, namely free-volume softening, thermal softening and coupling softening, are clearly revealed. The shear-banding instability originating from sole free-volume softening takes place *easier and faster* than that due to sole thermal softening, and dominates in the coupling softening. Furthermore, the coupled thermo-mechanical shear-band analysis does show that an initial slight distribution of local free volume can incur significant strain localization, producing a shear band. During such a localization process, the local free-volume creation occurs indeed *prior to* the increase in local temperature, indicating that the former is the cause of shear localization, whereas the latter is its consequence. Finally, extension of the above model to include the shear-induced dilatation shows that such dilatation facilitates the shear instability in metallic glasses.

1. Introduction

Earlier, Turnbull and Cech (1950) predicted that glass formation in liquid metals is possible if cooling is sufficiently fast and crystallization does not occur. Several years later, Klement et al. (1960) confirmed Turnbull's prediction by producing the first metallic glass from a liquid alloy of Au–Si. Since then, there have been extensive progresses in exploring metallic glasses (Chen, 1974; Pampillo, 1975; Drehman et al., 1982) and developing bulk metallic glasses (BMGs) with characteristic size in excess of 1 mm (Inoue et al., 1989; Peker and Johnson, 1993). The advent of more and larger BMGs arouses a revival of interests in the basic science of glass transition, glass structure, and their absorbing and potentially valuable properties (Greer, 1995; Johnson, 1999; Inoue, 2000; Wang et al., 2004; Schuh et al., 2007; Eckert et al., 2007). The long-range disorder in BMGs dictates their impressive array of mechanical properties, including extraordinary strengths (~1–5 GPa), high hardness (~2–12 GPa), large elastic deflections (~2% elastic strain) and relatively high fracture toughness (Lewandowski et al., 2005; Johnson and Samwer, 2005; Wang, 2006; Ashby and Greer, 2006), making them attractive candidates for many potential applications (Conner et al., 2000; Grimberg et al., 2006; Kumar et al., 2009). However, the major mechanical

* Corresponding author. Tel.: +86 10 82543958; fax: +86 10 82543977.
E-mail addresses: mqjiang@imech.ac.cn (M.Q. Jiang), lhdai@lnm.imech.ac.cn (L.H. Dai).

0022-5096/$ - see front matter © 2009 Elsevier Ltd. All rights reserved.
doi:10.1016/j.jmps.2009.04.008

shortcoming of BMGs is their limited room-temperature ductility, resulting from initiation and rapid propagation of a *single* shear band with characteristic thickness of ~10 nm (Donovan and Stobbs, 1981; Hufnagel et al., 2000; Li et al., 2002; Zhang and Greer, 2006a; Liu et al., 2005a, 2006; Jiang et al., 2009a). Brittleness is regarded as an intrinsic defect of metallic glasses. On the other hand, the formation of *multiple* shear bands throughout a sample, by controlled introduction of residual stress (Zhang et al., 2006b), modification of material composites (Schroers and Johnson, 2004; Das et al., 2005; Liu et al., 2007; Chen et al., 2008) and internal reinforcements by nano- or micro-particles and/or phases (Hays et al., 2000; Hofmann et al., 2008), is needed for enhancing its ductility. Therefore, clarifying the initiation or origin of shear-banding instability, as the crucial step to understand the whole shear-band process, in BMGs is of practical significance.

In polycrystalline alloys, the initiation of shear bands is attributed to local thermal softening (Zener and Hollomon, 1944; Bai and Dodd, 1992; Meyers, 1994; Wright, 2002; Zhang and Clifton, 2003; Chichili et al., 2004; Dai et al., 2004; Zhou et al., 2006). The critical conditions for the onset of such adiabatic shear bands (ASBs) have been studied extensively and well understood (Bai, 1982; Clifton et al., 1984; Molinari, 1997). As for metallic glasses, there have been two potential causes for the onset of shear-band instability, namely, mechanical initiation and thermal initiation. The first suggests that shear-induced dilatation causes the production of free volume, leading to a precipitous drop in viscosity within the shear band. This idea originates in the work of Spaepen (1977), who developed a steady-state inhomogeneous flow model based on a competition between stress-driven creation and diffusion annihilation of free volume. Subsequent works from Argon (1979), Steif et al. (1982), Vaks (1991), Falk and Langer (1998), and Wright et al. (2003) have also shown the importance of free-volume dynamics to shear instability. Recently, Huang et al. (2002) developed a general theoretical framework to characterize the inhomogeneous deformation in metallic glasses. In their work, the onset condition for shear instability is due to the sole effect of free volume. Note that these authors consider the shear-banding formation as an *isothermal* process. The second contends that the shear-banding event in BMGs is thermal-initiated, similar to ASBs in crystalline alloys (Leamy et al., 1972; Liu et al., 1998). A highway to investigate such hypothesis is the determination of temperature increase within the shear band. But this has long been controversial, with both measurements and predictions suggesting a wide range of values, from less than 0.1 K to a few thousand kelvins (Pampillo, 1975; Bengus et al., 1993; Liu et al., 1998; Wright et al., 2001; Hufnagel et al., 2002; Liu et al., 2005a; Lewandowski and Greer, 2006), which depends on different spatial and temporal resolutions. Despite the indeterminacy, the local heating is believed to remain important to shear-band instability (Yang et al., 2005; Zhang et al., 2007, 2008) and subsequent fracture process (Yang et al., 2006a), especially under dynamic loading. Recently, more and more works have indicated that the deformation of metallic glass is a thermo-mechanical process (Dai et al., 2005; Gao et al., 2007; Yang et al., 2006b; Thamburaja and Ekambaram, 2007; Zhang et al., 2007, 2008). If the applied stress and rate of deformation are high enough, both creation of free volume driven by stress and significant increase in temperature due to the dissipation of plastic work can occur and alter each other (Zhang et al., 2008). It is believed that the two physical processes are naturally coupled during the shear-banding formation in metallic glasses. In our previous work, the coupled effect of free-volume softening and thermal softening upon shear-banding instability in metallic glasses was discussed (Dai et al., 2005; Dai and Bai, 2008). Recently, Gao et al. (2007) argued for this coupled effect. Moreover, some coupled thermo-mechanical finite-deformation constitutive frameworks modeling the homogenous and/or inhomogenous flow in BMGs were also developed (Yang et al., 2006b; Thamburaja and Ekambaram, 2007). These coupled models provided some possible explanations for the experimental phenomena. However, for the physical origin of shear-banding instability, many basic questions have not been answered. In particular, during such a coupled process, is either of free-volume softening or thermal softening responsible for the onset of shear instability? How do the free volume and temperature interplay each other and what do they act as respectively? The key question "Must shear bands be hot?" is still pending and worth investigation (Spaepen, 2006).

To this end, we investigate the thermo-mechanical deformation of a bulk metallic glass undergoing one-dimensional simple shear. A viscoplastic constitutive law including two internal state variables, namely free-volume concentration and temperature, is provided. Homogeneous solution is obtained first. For the inhomogeneous mode, we perform a linear perturbation analysis based on the homogeneous solution; the onset criteria as well as the internal length and time scales of shear-banding instability are clearly revealed. In addition, a coupled thermo-mechanical shear-banding analysis is carried out, showing the process of strain localization. The effect of shear-induced dilatation on such shear instability is also discussed.

The scheme of this paper is as follows. Section 2 specifies the basic model within the context of continuum mechanics. The governing equations, including the constitutive equation, the momentum equation, the energy equation and the free-volume evolution equation, as well as the initial and boundary conditions for this problem are presented. In Section 3, we discuss three types of homogeneous deformations on the basis of the plastic flow rule developed by Spaepen (1977). In Sections 4 and 5, the linear perturbation analysis and shear-banding analysis are performed, respectively, to understand the inhomogeneous flow or shear-banding instability. In Section 6 we briefly discuss the effect of shear-induced dilatation on shear instability. Finally, conclusions and suggestions that deserve further investigations are given in Section 7.

2. The basic model

In this section we consider the thermo-mechanical deformation of a bulk metallic glass undergoing a simple shear. The problem is modeled as that of a planar layer infinitely extended in the shear direction x and in the out-of-plane direction z,

with finite height $2h$ in the y direction, as sketched in Fig. 1. The surfaces at $y=\pm h$ are sheared by applying constant velocities $\pm V_0$, parallel to the x-direction. Then, the deformation can be formulated in a one-dimensional framework; the variables depend solely on the coordinate y and the time t. Compared to the general form of constitutive law in conventional adiabatic shear problem, we adopt the following expression for the shear-stress depending on the strain and strain rate plus two internal state variables, i.e. temperature and free-volume concentration:

$$\tau=\psi(\gamma,\dot{\gamma},\theta,\xi), \tag{1}$$

where γ is the shear strain, $\dot{\gamma}=\partial\gamma/\partial t$ is the strain rate, θ the temperature, and ξ the concentration of free volume following Steif et al. (1982). Similar to the temperature, ξ is also a continuum field, being a function of position and time.

We assume that $\psi\geq 0$ for values of its arguments. For later use, let us introduce the notation

$$Q=\frac{\partial\psi}{\partial\gamma}>0 \quad \text{(strain hardening)}, \tag{2}$$

$$R=\frac{\partial\psi}{\partial\dot{\gamma}}>0 \quad \text{(strain rate hardening)}, \tag{3}$$

$$P=-\frac{\partial\psi}{\partial\theta}>0 \quad \text{(thermal softening)}, \tag{4}$$

$$F=-\frac{\partial\psi}{\partial\xi}>0 \quad \text{(free-volume softening)}. \tag{5}$$

Here, the strain hardening is expected to be valid for a short time immediately after yielding but before instability, considering that this study focuses on the initiation of shear instability. In accordance with continuum mechanics, the governing equations can be written in the following form:

$$\rho\frac{\partial\dot{\gamma}}{\partial t}=\frac{\partial^2\tau}{\partial y^2}, \tag{6}$$

$$\frac{\partial\theta}{\partial t}=\kappa\frac{\partial^2\theta}{\partial y^2}+A\tau\frac{\partial\gamma}{\partial t}, \tag{7}$$

$$\frac{\partial\xi}{\partial t}=D\frac{\partial^2\xi}{\partial y^2}+G(\xi,\theta,\tau), \tag{8}$$

where (6) is the Cauchy momentum equation, (7) the temperature evolution equation and (8) the free-volume evolution equation following Huang et al. (2002) and Dai et al. (2005); and κ the thermal diffusivity ($\kappa=\lambda/\rho C_v$, here λ, ρ and C_v being, respectively, the thermal conductivity, the mass density and the specific heat), A is a constant related to the Taylor–Quinney coefficient (β_{TQ}), given by $A=\beta_{TQ}/\rho C_v$, D is the diffusion coefficient of free-volume concentration, and $G(\xi,\theta,\tau)$ is the net generation rate of free volume, the explicit expression of which was presented by Spaepen (1977), as follows:

$$G(\tau,\xi,\theta)=\frac{1}{\chi}f\exp\left[-\frac{1}{\xi}\right]\exp\left[-\frac{\Delta G^m}{k_B\theta}\right]\left\{\frac{2k_B\theta}{\xi v^* S}\left[\cosh\left(\frac{\tau\Omega}{2k_B\theta}\right)-1\right]-\frac{1}{n_D}\right\}, \tag{9}$$

where χ is a geometrical factor, v^* the critical volume or the effective hard-sphere size of atom, f the frequency of atomic vibration (~Debye frequency), ΔG^m the activation energy, k_B is the Boltzmann constant, S the effective shear modulus

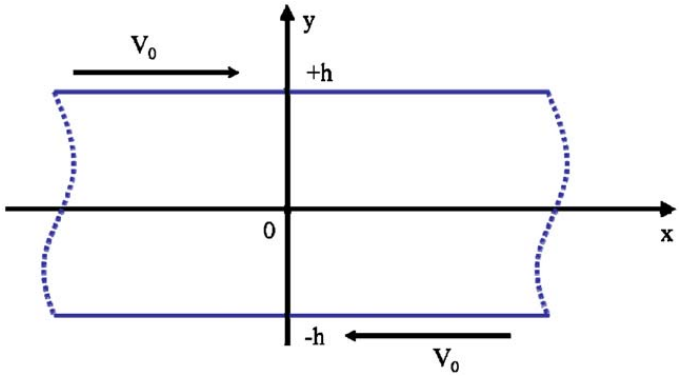

Fig. 1. Geometry of simple shearing of a planar bulk metallic glass body.

($S=2(1+\nu)\mu/3(1-\nu)$ with μ being the shear modulus and ν being Poisson's ratio), Ω the atomic volume and n_D the number of diffusive jumps necessary to annihilate a free volume equal to v^*. Eq. (8) states that there are three different physical processes that can alter the local free-volume concentration: diffusion, annihilation and generation. The free volume can be redistributed by diffusion until it is spatially uniform. The metastable state of metallic glass allows free volume to annihilate at any position simply by the atomic rearrangement. In addition, the generation of free volume is induced by stresses. Since G is a function of τ, θ, and ξ, we can also define the following parameters:

$$G^{\xi}=\frac{\partial G}{\partial \xi}, \tag{10}$$

$$G^{\theta}=\frac{\partial G}{\partial \theta}, \tag{11}$$

$$G^{\tau}=\frac{\partial G}{\partial \tau}, \tag{12}$$

for later analysis. Eqs. (10)–(12) characterize the net creation rate of free volume due to itself, temperature and shear stress, respectively.

The compatibility equation is

$$\frac{\partial \gamma}{\partial t}=\frac{\partial V}{\partial y}, \tag{13}$$

where V is the particle velocity in the x-direction.

The initial condition (IC) and the boundary condition (BC) governing the one-dimensional simple shearing are given by

$$IC\begin{cases}\gamma(y,0)=0, & \dot{\gamma}(y,0)=\dfrac{V_0}{h},\\ \theta(y,0)=\theta_i, & \xi(y,0)=\xi_i,\end{cases} \tag{14}$$

where the initial temperature θ_i is taken as 300 K, and the initial free-volume concentration $\xi_i=0.05$ following Huang et al. (2002) and Gao et al. (2007) and

$$BC\begin{cases}\gamma(\pm h,t)=\dfrac{V_0}{h}t,\\ \dot{\gamma}(\pm h,t)=\dfrac{V_0}{h},\\ \dfrac{\partial\theta(\pm h,t)}{\partial y}=0,\\ \dfrac{\partial\xi(\pm h,t)}{\partial y}=0.\end{cases} \tag{15}$$

Here, in order to highlight the essential physics, the adiabatic boundary conditions are assumed for all strain rates for simplicity, even under low strain rate following Gao et al. (2007). If the specific form of constitutive relation (1) is determined, we can solve simultaneously the coupled governing Eqs. (1), (6)–(9) and (13)–(15) for the fields of shear stress, shear strain, temperature and free-volume concentration at any time.

3. Homogeneous deformation

Shear-banding formation is a result of the instability of homogeneous deformation. In addition, the deformation within a shear band can be approximately regarded as a highly localized homogeneous deformation (Argon, 1979; Steif et al., 1982). Therefore, it is important to seek homogeneous solutions by assuming that

$$\frac{\partial \tau}{\partial y}=\frac{\partial \theta}{\partial y}=\frac{\partial \xi}{\partial y}=0. \tag{16}$$

This means that the shear strain, the shear stress, the free-volume concentration and the temperature are uniformly distributed within the material. Then, the governing equations become

$$\tau_h=\psi(\gamma_h,\dot{\gamma}_h,\theta_h,\xi_h), \tag{17}$$

$$\frac{\mathrm{d}\dot{\gamma}_h(t)}{\mathrm{d}t}=0, \tag{18}$$

$$\frac{\mathrm{d}\theta_h(t)}{\mathrm{d}t}=A\tau_h\dot{\gamma}_h, \tag{19}$$

$$\frac{d\xi_h(t)}{dt} = G(\tau_h, \theta_h, \xi_h). \tag{20}$$

The Cauchy strain γ can be decomposed into elastic and plastic parts, which are assumed to be decouple for simplicity, so that

$$\gamma = \gamma^e + \gamma^p, \tag{21}$$

where the elastic strain γ^e obeys Hooke's law

$$\gamma^e = \frac{\tau}{\mu}. \tag{22}$$

The microscopic mechanism that governs homogeneous plastic flow in metallic glasses has been discussed by Spaepen (1977). Macroscopic flow is modeled as occurring as a result of a number of individual atom jumps each contributing to a small local shear strain. The flow rule or the plastic strain rate $\dot{\gamma}^p$ is given as follows:

$$\begin{aligned}\dot{\gamma}^p = &(\text{strain produced at each site})\\ &\times(\text{fraction of potential jump sites})\\ &\times(\text{net number of forward jumps at each site per second}).\end{aligned} \tag{23}$$

Within the free-volume formalism, Eq. (23) can be written as

$$\dot{\gamma}^p = 2f\exp\left(-\frac{\Delta G^m}{k_B\theta}\right)\sinh\left(\frac{\tau\Omega}{2k_B\theta}\right)\exp\left(-\frac{1}{\bar{\xi}}\right). \tag{24}$$

The constitutive relation (17) modeling a metallic glass undergoing homogeneous shearing is then of the following form:

$$\dot{\tau} = \mu\left[\dot{\gamma} - 2f\exp\left(-\frac{\Delta G^m}{k_B\theta}\right)\sinh\left(\frac{\tau\Omega}{2k_B\theta}\right)\exp\left(-\frac{1}{\bar{\xi}}\right)\right]. \tag{25}$$

In order to examine the respective effect of temperature and free volume, we purposely discuss three types of homogeneous deformations: (I) *Isoconfigurational deformation*, during which temperature evolves with time, but free volume keeps constant (i.e. only Eqs. (17)–(19) are considered); (II) *Isothermal deformation*, during which free volume changes, but temperature is constant (i.e. only Eqs. (17), (18) and (20) are included); and (III) *Coupling deformation*, considering the interplay between temperature and free volume. The three homogeneous deformations therefore lead to three types of shear-banding instability: *thermal softening*, *free-volume softening* and *coupling softening*, respectively, which we will clarify in Section 4.

In addition, we focus on the four governing parameters that are very important to intuitively understand shear-banding instability from the homogeneous solution. They are defined as follows:

(a) *Viscosity*, defined as

$$\eta = \frac{\tau_h}{\dot{\gamma}_h^p}. \tag{26}$$

(b) *Deborah number*. In the field of rheology, the so-called Deborah number plays an important role, since it describes the influence of time on the observed flow properties (Moura-Ramos and Correia, 2001). In some sense, glass is "frozen" liquid that has lost its ability of flow or mobility. During deformation, metallic glasses can behave as liquid or solid. This flow and deformation behavior can be characterized by a dimensionless Deborah number (Reiner, 1964), defined as

$$D_e = \frac{t_r}{t_e}, \tag{27}$$

where $t_r = \eta/\mu$ is the Maxwell time or internal structural relaxation time under loading and $t_e = \gamma/\dot{\gamma}$ is the macroscopic imposed time of external loading. The magnitude of the Deborah number, D_e, provides interesting indications. If t_e is very large compared with the relaxation time t_r, we see metallic glasses behaving as an ordinary viscous fluid. However, in the opposite case, they behave as a glassy solid. Thus, the smaller the D_e is, the more liquid-like the metallic glass behaves.

(c) *The thermal instability index*. As carried out by Gao et al. (2007), we introduce an instability index due to local temperature increase, defined as

$$IN_\theta = \frac{\partial f_h}{\partial \theta_h}, \tag{28}$$

where $f_h = A\tau_h\dot{\gamma}^p$ is the temperature rising rate due to the plastic work converting to heat. Thus, IN_θ measures how fast the temperature increases.

Table 1
Mechanical properties and parameters for Vit 1.

Properties and parameters	Notation	Value
Shear modulus	μ	35.3 GPa
Poisson ratio	ν	0.36
Density	ρ	6125 kg m^{-3}
Specific heat at constant volume	C_v	400 J kg^{-1} K^{-1} or $C_v(\theta)$
Tayor–Quinney coefficient	β_{TQ}	0.9 or $\beta_{TQ}(\dot{\gamma})$
Thermal conductivity	λ	20 W m^{-1} K^{-1}
Free-volume diffusivity	D	$\sim 10^{-16}$ m^2 s^{-1}
Average atomic volume	Ω	20A^3
Activation energy	ΔG^m	0.2–0.5 eV
Debye temperature	θ_D	327 K
Frequency of atomic vibration	f	$\sim 10^{13}$ s^{-1}

(d) *The free-volume instability index*. In parallel, an instability index due to free-volume creation can be defined as

$$IN_\xi = \frac{\partial G_h}{\partial \xi_h}. \tag{29}$$

This index characterizes the speed of the free-volume creation. Compared to Eq. (10), IN_ξ is indeed equal to ${G_h}^\xi$.

We now select suitable material parameters for calculation. For the sake of comparison with relevant results (e.g., Steif et al., 1982; Huang et al., 2002; Gao et al., 2007; Yang et al., 2006a), we take a typical $Zr_{41.2}Ti_{13.8}Cu_{10}Ni_{12.5}Be_{22.5}$ (Vit 1) BMG as a model material. The physical properties for Vit 1 used in our paper are mostly derived from these literatures and listed in Table 1. To better understand numerical results, guided by Steif et al. (1982) and Gao et al. (2007), we introduce the reference physical quantities as follows:

$$\text{temperature } \theta_0 = 300\,\text{K}, \tag{30}$$

$$\text{stress } \tau_0 = \frac{2k_B\theta_0}{\Omega} \sim 414\,\text{MPa}, \tag{31}$$

$$\text{time } t_0 = f^{-1}\exp\left(\frac{\Delta G^m}{k_B\theta_0}\right) \sim 10^{-5}\,\text{s} \tag{32}$$

to normalize the governing equations. Then, we obtain some dimensionless variables as follows: temperature $\tilde{\theta} = \theta/\theta_0$; shear stress $\tilde{\tau} = \tau/\tau_0$ or shear modulus $\tilde{\mu} = \mu/\tau_0$; shear strain rate $\tilde{\dot{\gamma}} = \dot{\gamma}t_0$ or time $\tilde{t} = t/t_0$. Throughout this paper, when dimensional and non-dimensional quantities are to be distinguished, any variable with an over tilde ($\sim$) will be dimensionless. In the case of homogeneous deformation, the total strain rate $\dot{\gamma}$ is regarded as a prescribed constant with a typical value of 10^{-2} s^{-1}, corresponding to $\tilde{\dot{\gamma}} = 10^{-7}$, over the deformation history. In what follows, if no specific state, all calculations are under this strain rate. According to Eq. (18), the shear strain increases γ_h linearly with time at the constant strain rate. τ_h, θ_h and ξ_h can be obtained by numerically integrating Eqs. (19), (20) and (25). Based on the obtained homogeneous solution, the material parameters defined in Section 1, that is Q_h, R_h, P_h, F_h, ${G_h}^\xi$, ${G_h}^\tau$ and ${G_h}^\theta$, as well as the four governing variables (η, D_e, IN_θ and IN_ξ) can be also calculated.

Fig. 2 shows the homogeneous solution at $\dot{\gamma} = 10^{-2}$ s^{-1} for the three typical cases. The normalized shear stress, the free-volume concentration and the normalized temperature versus shear strain are, respectively, illustrated in Fig. 2a–c. For isoconfigurational deformation, an initial elastic response is followed by a gradual drop in stress, during which the temperature increases by inches with plasticity developing (see Fig. 2c). After the peak stress corresponding to $\gamma \approx 0.07$, there is a continuing strain softening, resulting in final failure. As for the isothermal and the coupling deformations, the plastic parts exhibit some different features. First, the plastic yielding occurs earlier, followed by a precipitous drop in stress. Second, the peak stress is lower than the isoconfigurational one, implying the isoconfigurational activation energy softening the material be greater than that in the isothermal or coupling case. The result agrees well with the experimental measures (Taub and Spaepen, 1980). Combining Fig. 2a with Fig. 2b, we find that in the early stage of deformation (shear strain of 0–0.05), the shear stress is relatively low and cannot drive the generation of free volume. However, the annihilation of free volume still occurs due to the presence of an initial temperature of 300 K (or normalized temperature of 1.0). This results in a slight decrease in the free-volume concentration at the beginning. With the applied load increasing further, the creation rate exceeds the annihilation rate, leading to a drastic rise in the free-volume concentration. At the same time, the net increase of free volume, in turn, results in a catastrophic drop in shear stress. In the isothermal case, the annihilation rate, eventually, balances the creation rate, and a steady-state free volume has been achieved at which the shear stress stays constant. However, in the coupling case, the presence of temperature, on the one hand, facilitates the faster creation of free volume (see inset to Fig. 2b) before yielding. On the other hand, the temperature rise, in favor of the annihilation of free volume, decreases the total amount of free volume, after yielding occurs. The significant decrease of

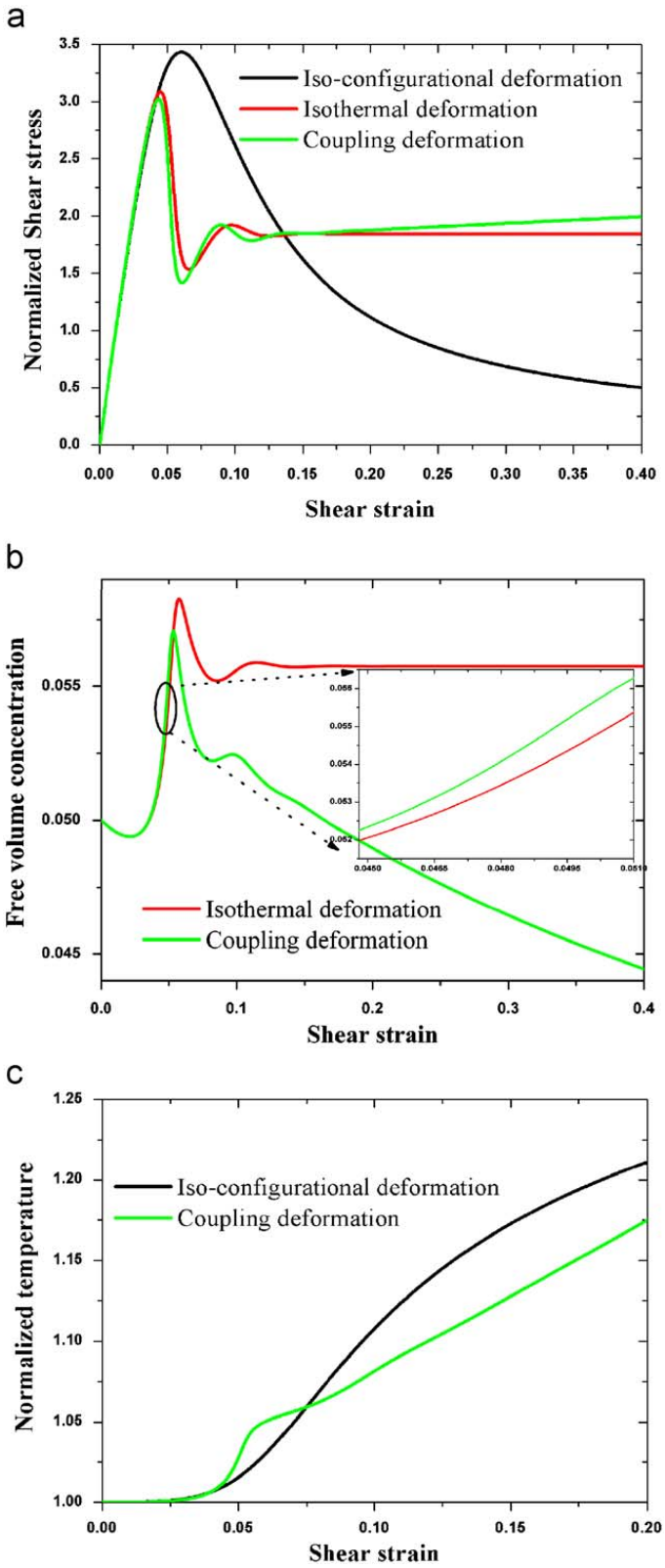

Fig. 2. The solution of homogeneous deformation at strain rate $\dot{\gamma} = 10^{-2}\,s^{-1}$: (a) normalized shear stress τ/τ_0, (b) free-volume concentration ξ, and (c) normalized temperature θ/θ_0 versus shear strain γ.

free-volume concentration at the late stage of deformation (above 0.1 shear strain) can result in considerable increase in shear stress or strain hardening, compensating for the significant strain softening due to the temperature increase. Finally, only a slight strain hardening occurs compared to the isothermal deformation case. In addition, it is easily noted from Fig. 2c that the drastic increase in free volume causes more remarkable instantaneous temperature rise at yielding point.

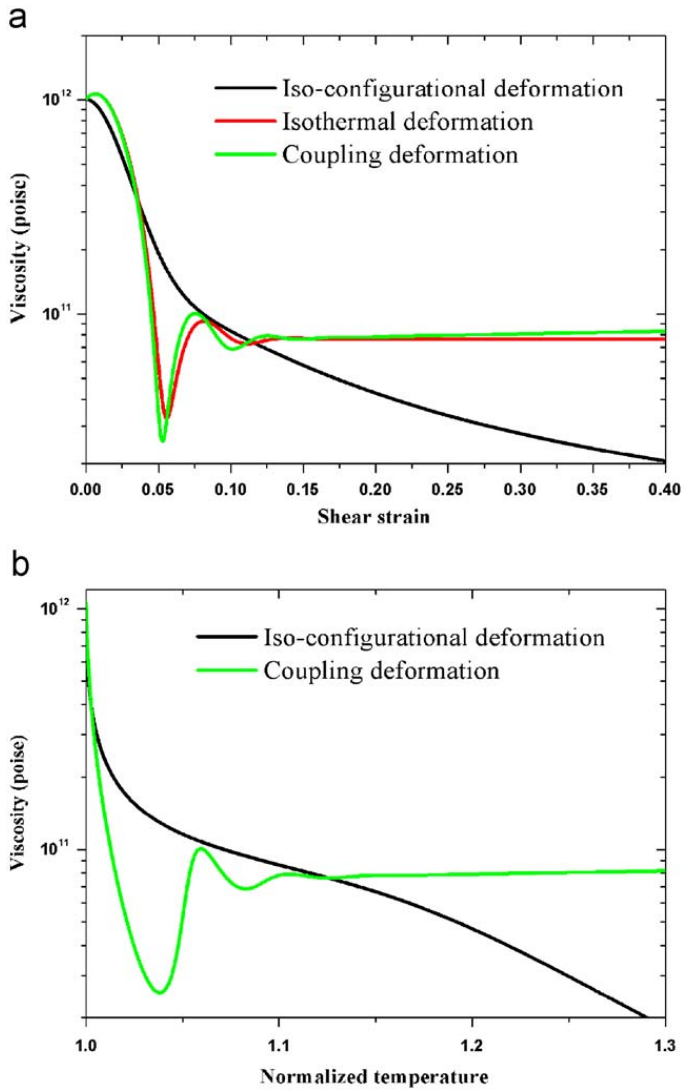

Fig. 3. The viscosity as a function of (a) the applied shear strain and (b) normalized temperature.

The viscosity defined in Eq. (26) as a function of shear strain is shown in Fig. 3a. It is clearly seen that both temperature and free volume can decrease the viscosity and hence soften materials. But before plastic yielding occurs, the decrease in viscosity due to free-volume increase is much faster than that due to temperature increase. In addition, a lower value of viscosity is achieved in the cases taking free volume into account. Fig. 3b gives the viscosity–temperature relations during homogeneous deformation. In the isoconfigurational state, the viscosity decreases monotonously and slowly with increase in temperature. In the temperature–free-volume coupling case, an initial precipitous decrease in viscosity is followed by a drastic rebound prior to a steady state. Obviously, this behavior is mainly determined by free volume instead of temperature. The free volume decreases the viscosity much faster than the temperature during the early stage of deformation, which gives states that are less viscous than the isoconfigurational state at the same temperature. So, it seems that the free-volume creation provides an easier way to initiate instability than temperature increase. It should be pointed out that the slight increase in viscosity at the late stage of deformation in the coupling case is also a compound result of both free-volume decrease and temperature increase. The variation of Deborah number with shear strain, as shown in Fig. 4, gives the results consistent with Fig. 3. The free-volume creation prior to a steady state will lead to a relatively smaller Deborah number, which is indicative of more liquid-like states.

Fig. 5a gives the variations of the thermal instability index IN_θ, defined as Eq. (28), with shear strain under the strain rate of $10^{-2}\,s^{-1}$. According to its physical meaning, the curve peak corresponds to a potential instability point due to the temperature increase. In the isoconfigurational case, the IN_θ curve shows a broad crest with a maximum of ~0.02. In contrast, the coupling case, with the participation of free volume, exhibits two distinct features: (i) the maximum value of IN_θ is almost double, which indicates that the creation of free volume promotes the increase in temperature; (ii) the peak is much more precipitous and narrower, implying a much higher localized instability. For these two cases, the peak value max[IN_θ] increases with increasing strain rate, as shown in Fig. 5b. In addition, the difference in the maximum becomes

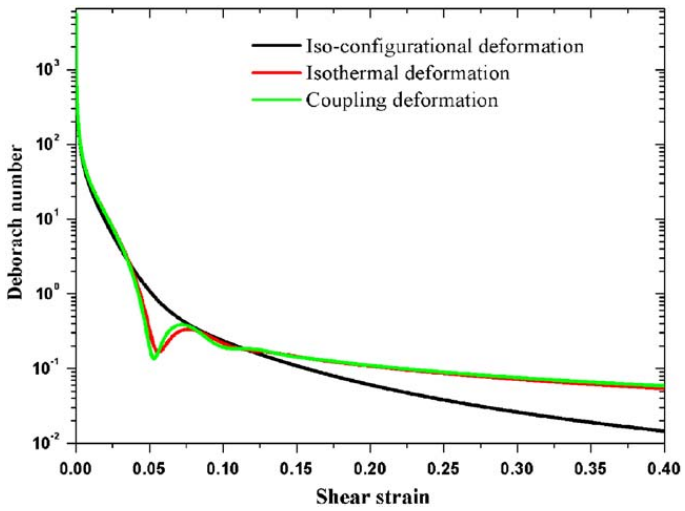

Fig. 4. Variation of Deborah number with shear strain from the homogeneous solution.

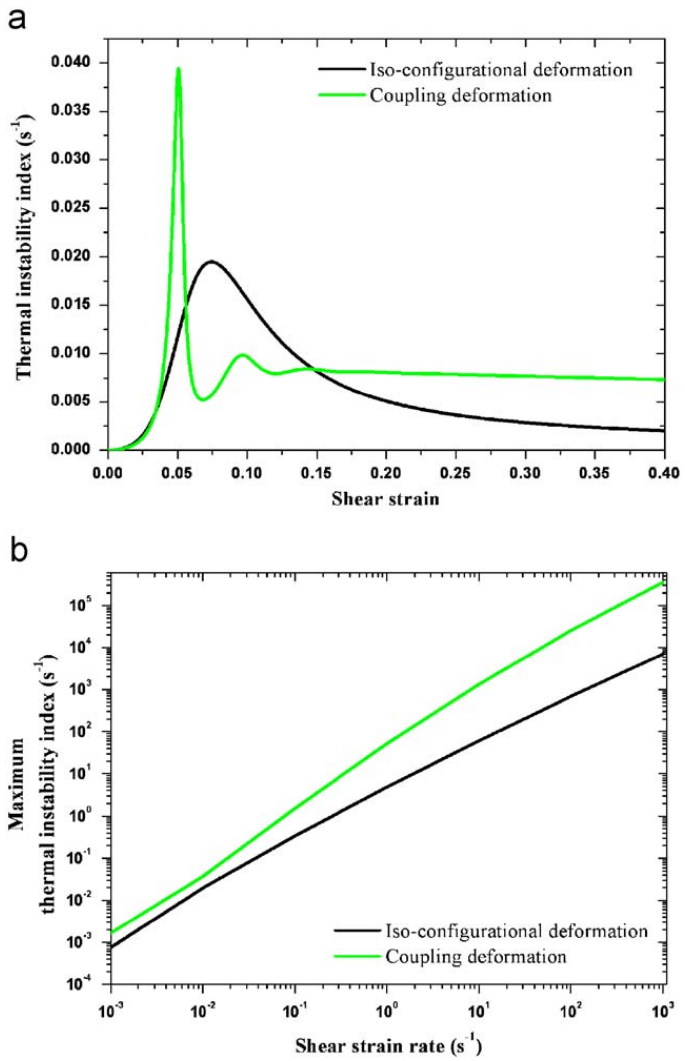

Fig. 5. (a) Change of thermal instability index with shear strain and (b) maximum thermal instability index versus applied shear strain rate.

more remarkable with increase in strain rates. This implies that, in the coupling case, a much faster temperature increase occurs because of the presence of free-volume creation under higher loading rates. The free-volume instability index IN_{ξ}, defined as Eq. (29), evolving with shear strain is plotted in Fig. 6a. Overall, the shapes of two curves are similar. However,

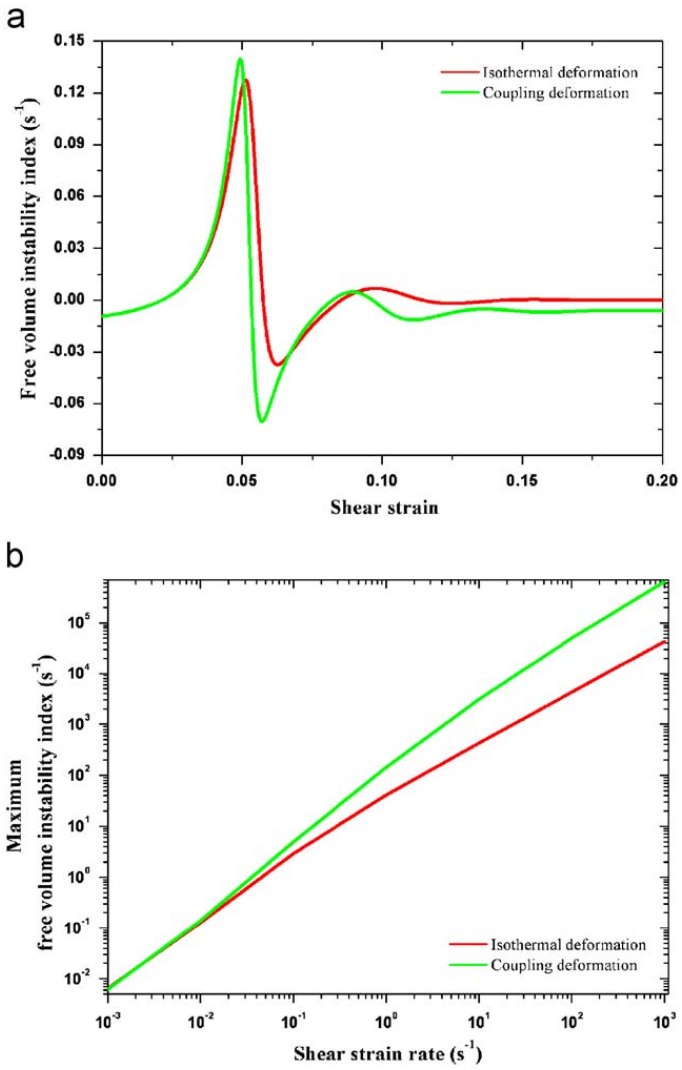

Fig. 6. (a) Change of free-volume instability index with shear strain and (b) maximum free-volume instability index versus applied shear strain rate.

the presence of temperature causes a slightly higher maximum value and a much smaller minimum. This two-edged effect of temperature increase on the free-volume concentration is consistent with the results in Fig. 2b. In detail, the increase in temperature speeds up the free-volume creation before instability, while slowing down its creation after instability. In analogy with IN_θ, the maximum value max[IN_ξ] of free-volume instability index also depends on the prescribed strain rate, as shown in Fig. 6b. Higher strain rates can induce higher max[IN_ξ] in both isothermal and coupling deformation. Besides, the temperature increase due to dynamic loading makes for the instantaneous free-volume increase, leading to higher max[IN_ξ]. Comparing results in Fig. 5a with Fig. 6a, we find that max[IN_ξ] is some one order of magnitude higher than max[IN_θ] in the coupling case. This indicates that the stress-driven instantaneous free volume creates more rapidly than the instantaneous temperature increase. The aforementioned homogeneous deformation uncovered clearly some crucial information during the pre-instability process, as follows:

(1) The creation of free volume is accompanied with a sudden temperature rising. The temperature rise, on the one hand, speeds up the free-volume creation before yielding, and on the other hand, decreases the total amount of free volume after yielding.
(2) Material softening due to the free-volume creation is much easier than that due to temperature increasing, since the free volume increases much faster than the instantaneous temperature rise.

4. Linear perturbation analysis and inherent scales

Shear banding, a physically unstable event, can be regarded as the appearance of mathematical instability in the differential equations governing the inhomogeneous deformation. Usually, the stability analysis is simplified by seeking an

inhomogeneous deformation solution with respect to small perturbations on the homogeneous solution. Examples of this dealing can be found in Bai (1982), Clifton et al. (1984), Molinari (1997), Huang et al. (2002), Dai et al. (2005) and Gao et al. (2007). Of great interest is the origin of instability; hence, the linear perturbation analysis is valid.

To linearize problems (1) and (6)–(8) about the homogeneous solution (17)–(20), we impose a perturbation $(\delta\tau, \delta\gamma, \delta\theta, \delta\xi)$ on the time-dependent homogeneous solution $(\tau_h, \gamma_h, \theta_h, \xi_h)$, such that

$$\tau(y,t) = \tau_h + \delta\tau(y,t), \tag{33}$$

$$\gamma(y,t) = \gamma_h + \delta\gamma(y,t), \tag{34}$$

$$\theta(y,t) = \theta_h + \delta\theta(y,t), \tag{35}$$

$$\xi(y,t) = \xi_h + \delta\xi(y,t). \tag{36}$$

They are the inhomogeneous solutions of (1) and (6)–(8). In order to render the mathematical derivation tractable, here we apply a perturbation to shear stress in advance. For all practical purposes, $(\tau_h, \gamma_h, \theta_h, \xi_h)$ are assumed to vary slowly with time as compared to $(\delta\tau, \delta\gamma, \delta\theta, \delta\xi)$ so that $(\tau_h, \gamma_h, \theta_h, \xi_h)$ can be considered as constant during the inhomogeneous deformation. Hence, the calculated parameters based on the homogeneous solution also keep constant.

The perturbation has the following form:

$$\delta\tau = \tau_* \exp(\alpha t + iky), \tag{37}$$

$$\delta\gamma = \gamma_* \exp(\alpha t + iky), \tag{38}$$

$$\delta\theta = \theta_* \exp(\alpha t + iky), \tag{39}$$

$$\delta\xi = \xi_* \exp(\alpha t + iky), \tag{40}$$

where $(\tau_*, \gamma_*, \theta_*, \xi_*)$ are small constants that characterize the initial magnitude of the perturbation, k is the wave number and α related to the initial rate of growth. The stability of the deformation is now determined by the sign of the real part of α: if $\mathrm{Re}(\alpha)<0$, the shear deformation is stable; if $\mathrm{Re}(\alpha)>0$, it is unstable.

Introducing Eqs. (33)–(40) into Eqs. (1) and (6)–(8) and only considering terms that are of first order in $(\delta\tau, \delta\gamma, \delta\theta, \delta\xi)$ yields

$$\mathbf{C}\cdot\mathbf{S} = \mathbf{0}, \tag{41}$$

where

$$\mathbf{C} = \begin{bmatrix} \rho\alpha^2 + k^2(Q_h + \alpha R_h) & -k^2 P_h & -k^2 F_h \\ A[\alpha\tau_h + \dot{\gamma}_h(Q_h + \alpha R_h)] & -(A\dot{\gamma}_h P_h + \alpha + \kappa k^2) & -A\dot{\gamma}_h F_h \\ G_h^\tau(Q_h + \alpha R_h) & G_h^\theta - P_h G_h^\tau & G_h^\xi - \alpha - Dk^2 - F_h G_h^\tau \end{bmatrix} \tag{42}$$

and

$$\mathbf{S} = \begin{bmatrix} \gamma_* \\ \theta_* \\ \xi_* \end{bmatrix}. \tag{43}$$

To have a non-trivial solution, the determinant of matrix $\mathbf{C}$ must be equal to zero, that is

$$|\mathbf{C}| = 0. \tag{44}$$

This leads to the spectral equation for the initial growth rate α of the perturbation:

$$a_4\alpha^4 + a_3\alpha^3 + a_2\alpha^2 + a_1\alpha^1 + a_0 = 0. \tag{45}$$

The coefficients of this polynomial are defined by

$$a_4 = 1, \tag{46}$$

$$a_3 = \Gamma_1 + \Gamma_2 + G_h^\tau F_h, \tag{47}$$

$$a_2 = \frac{k^2}{\rho}\Gamma_3 + \Gamma_1\Gamma_2 + \kappa G_h^\tau F_h k^2 + A\dot{\gamma}_h G_h^\theta F_h, \tag{48}$$

$$a_1 = \frac{k^2}{\rho}(\Gamma_2\Gamma_3 + \kappa Q_h k^2 - A\tau_h G_h^\theta F_h), \tag{49}$$

$$a_0 = \frac{k^4}{\rho}\kappa Q_h \Gamma_2, \tag{50}$$

where

$$\Gamma_1 = (\kappa + \nu)k^2 + A\dot{\gamma}_h P_h, \tag{51}$$

$$\Gamma_2 = Dk^2 - G_\xi, \tag{52}$$

$$\Gamma_3 = \kappa R_h k^2 + Q_h - A\tau_h P_h \tag{53}$$

with $\nu = R_h/\rho$, which can be considered as the momentum or viscosity diffusion coefficient. Usually, $\nu \geq 10^2\,\mathrm{m^2\,s^{-1}}$ in metallic glasses. So, we have $\nu \gg \kappa \gg D$.

Thus, the question of stability of the linearized problem becomes basically algebraic in nature and investigates the signs of the real part of the roots of spectral Eq. (45). According to the well-known Routh–Hurwitz criterion (Sanchez, 1968), if

$$\begin{cases} a_3 > 0, \\ a_3 a_2 - a_1 > 0, \\ (a_3 a_2 - a_1)a_1 - a_3^2 a_0 > 0, \\ a_0 > 0 \end{cases} \tag{54}$$

then all roots of (45) have negative real parts, indicating stable deformation. If the reverse of (54) is true, the system will be unstable. We now use this criterion to analyze the three types of instability: (I) thermal softening, (II) free-volume softening and (III) coupling softening, which were defined in Section 3.

(I) *Thermal softening*. If we consider only thermal softening by eliminating the third row and column in matrix **C**, then the coefficients of spectral Eq. (45) become

$$a_4 = 0, \tag{55}$$

$$a_3 = 1, \tag{56}$$

$$a_2 = k^2(\kappa + \nu) + A\dot{\gamma}_h P_h, \tag{57}$$

$$a_1 = k^4 \kappa\nu + \frac{k^2}{\rho}(Q_h - A\tau_h P_h), \tag{58}$$

$$a_0 = \frac{k^4}{\rho}\kappa Q_h. \tag{59}$$

In fact, the spectral Eq. (45) degenerates into a cubic equation in this case. We find from (54) that a root of (45) can have a real part greater than zero, when $k \neq 0$, if and only if

$$\frac{A\tau_h P_h}{Q_h} > 1 + \frac{R_h}{Q_h}\kappa k^2 \tag{60}$$

or

$$A\tau_h P_h > Q_h + R_h \kappa k^2. \tag{61}$$

Note that $\nu \gg \kappa$ is used in deriving this inequality that is the general criterion for instability due to thermal softening. This criterion expresses a basic competition between the stabilizing effects of strain hardening Q_h, strain-rate-hardening R_h, thermal diffusion κ and the destabilizing effect of thermal-softening P_h. If the deformation is adiabatic, i.e. $\kappa \to 0$, the instability criterion (60) then simplifies to

$$\frac{A\tau_h P_h}{Q_h} > 1. \tag{62}$$

Actually, $A\tau_h P_h/Q_h$ is the dimensionless variable B, defined by Bai (1982). Inequality (62) is totally identical to that of the classical adiabatic shear instability for crystalline materials where thermal softening is the sole factor resulting in instability (Bai, 1982). Regarding the role of wave number or the perturbation per se on instability, there are two extreme situations

(a) For small-wavelength limit ($k \to \infty$), the spectral Eq. (45) becomes

$$\frac{R_h}{Q_h}\alpha + 1 = 0, \tag{63}$$

where only terms that are of the highest order in k are considered. The only solution of (63) is

$$\alpha = -\frac{Q_h}{R_h} < 0. \tag{64}$$

Then it is deduced that shear deformation is always stable. In this case, the enhanced thermal diffusion,$\kappa k^2 \to \infty$, restrains the growth of perturbation (Molinari, 1997; Grady, 1992).

(b) For long-wavelength limit ($k \to 0$), the spectral Eq. (45) simplifies to

$$\alpha(\alpha + A\dot{\gamma}_h P_h) = 0. \tag{65}$$

Its solutions are

$$\alpha = 0 \ \text{ or } \ \alpha = -A\dot{\gamma}_h P_h < 0. \tag{66}$$

Shear deformation is again always stable, which contributes to the accelerated diffusion of momentum (inertia), $R_h \to \infty$, under $k \to 0$ (Molinari, 1997; Grady, 1992). The results imply that there is an optimal wave number or length scale related to shear-band thickness or spacing in adiabatic shear instability, which properly balances thermal and momentum diffusion.

According to inequality (60), we can define a critical wavelength ℓ_θ, which is the internal thermal length scale, of thermal softening instability, as follows:

$$\ell_\theta = 2\pi\left(\frac{R_h \kappa}{A\tau_h P_h - Q_h}\right)^{1/2}. \tag{67}$$

Perturbations with a wavelength smaller than ℓ_θ will die out, and the ones with a wavelength larger than ℓ_θ will grow exponentially. However, the instability must occur at a special set of wavelength or wave number, which is the dominant mode instability. This wavelength k_m corresponds to the maximum growth rate α_m of perturbations. In addition to the spectral Eqs. (45) and (55)–(59), k_m and α_m have to satisfy the extremum condition

$$\frac{\mathrm{d}\alpha_m}{\mathrm{d}k_m} = 0, \tag{68}$$

that is,

$$k_m^2 = \frac{(A\tau_h P_h/Q_h - 1)(\alpha_m/\kappa) - (1/\nu + 1/\kappa)(R_h/Q_h)\alpha_m^2}{2(1 + (R_h/Q_h)\alpha_m)}. \tag{69}$$

This is the dispersion equation in the dominant modes due to thermal softening. Due to ${k_m}^2 \geq 0$, we arrive at the upper-bound estimate of α_m

$$\alpha_m \sim \frac{A\tau_h P_h - Q_h}{R_h + \rho\kappa}. \tag{70}$$

Thus, we obtain the characteristic time of instability as follows:

$$t_\theta \sim \frac{1}{\alpha_m} = \frac{R_h + \rho\kappa}{A\tau_h P_h - Q_h}. \tag{71}$$

This time scale measures how fast perturbations will grow. So, it is reasonable to regard t_θ as the internal thermal time scale. In the adiabatic condition ($\kappa \to 0$), Eq. (71) degenerates into the result obtained by Bai (1982). Bear in mind that our main purpose is the initiation of instability. Therefore, we can use the internal length and time scales of instability to characterize whether the instability occurs easily or with difficulty.

(II) *Free-volume softening*. By this means eliminating the second row and column in matrix **C**, we can examine the sole effect of free volume on instability. In such a case, the coefficients of spectral Eq. (45) have the following form:

$$a_4 = 0, \tag{72}$$

$$a_3 = 1, \tag{73}$$

$$a_2 = -G_h^\xi + F_h G_h^\tau + (\nu + D)k^2, \tag{74}$$

$$a_1 = k^2\left[\nu(-G_h^\xi + Dk^2) + \frac{Q_h}{\rho}\right], \tag{75}$$

$$a_0 = \frac{Q_h}{\rho}k^2(-G_h^\xi + Dk^2). \tag{76}$$

By the Routh–Hurwitz criterion (54), the necessary and sufficient condition ($k\neq 0$) for instability is

$$G_h^{\xi} > Dk^2. \tag{77}$$

Note also that this instability criterion is totally identical to that derived by Huang et al. (2002). The underlying physics is that, if and only if the net creation of free volume is faster than its diffusion, perturbation will grow and deformation becomes unstable. The stability in system is only dominated by the competition between these two microscopic rate-dependent processes. The factors such as strain-hardening Q_h, strain-rate-hardening R_h and momentum diffusion ν are not related to the initiation of instability.

The two extreme situations about the wave number k can also be discussed

(a) For small-wavelength limit ($k\to\infty$), the spectral equation and its only solution are (63) and (64), respectively. Then, the deformation is again always stable, due to the stabilizing effect of free-volume diffusion, i.e. $Dk^2\to\infty$.

(b) For long-wavelength limit ($k\to 0$), the spectral Eq. (45) becomes

$$\alpha^2 + (F_h G_h^{\tau} - G_h^{\xi})\alpha = 0. \tag{78}$$

The solutions are

$$\alpha = 0 \ \text{ or } \ \alpha = G_h^{\xi} - F_h G_h^{\tau}. \tag{79}$$

Thus, perturbation will grow if and only if $G_h^{\xi} > F_h G_h^{\tau}$, implying that the system is not always stable when $k\to 0$. From a physical point of view, the shear band in BMGs initiates on a $\sim$10 nm scale compared to the length scale of the underlying local "flow event" at which the continuum momentum diffusion maybe is no longer valid. However, the ASB in crystalline alloys develops on a $\sim$100 μm scale at which momentum diffusion is still valid. The result indicates totally different instability mechanisms between thermal softening and free-volume softening.

According to (77), the balance of free-volume creation with diffusion will determine a critical wavelength ℓ_{ξ}, as follows:

$$\ell_{\xi} = 2\pi\left(\frac{D}{G_h^{\xi}}\right)^{1/2}. \tag{80}$$

This is the internal free-volume length scale, determining whether instability occurs or not. Moreover, we still investigate the dominant instability mode to look for the internal time scale. Combining spectral Eqs. (45), (72)–(76) and the extremum condition (68) leads to the dispersion equation:

$$k_m^2 = \frac{1}{2\nu}\left(G_h^{\xi} - \alpha_m - \frac{DR_h\alpha_m^2}{\nu(Q_h + R_h\alpha_m)}\right). \tag{81}$$

Considering ${k_m}^2 \geq 0$ and $\nu \gg D$, the upper-bound estimate of α_m is ${G_h}^{\xi}$; hence, the characteristic time of instability, which can be considered as the internal free-volume time scale t_{ξ}:

$$t_{\xi} \sim \frac{1}{G_h^{\xi}}. \tag{82}$$

Similar to t_{θ}, this internal time measures how fast the instability occurs in the free-volume softening case. It is noted from (82) that only the characteristic time for the free-volume creation is incorporated into the total time scale. The reason for this is that the free-volume diffuses much more slowly than its coalescence. However, the situation is just opposite in the case of thermal softening, where the thermal diffusion is much faster than thermal excitation. Therefore, high strain rates and low thermal conductivity are necessary to induce significant transient temperature rise.

(III) *Coupling softening*. The spectral equation and its coefficients are (45) and (46)–(50), respectively. According to the Routh–Hurwitz criterion (54), we obtain the onset condition for such instability:

$$G_h^{\xi} + \frac{A\tau_h G_h^{\theta} F_h - \kappa Q_h k^2}{\kappa R_h k^2 + Q_h - A\tau_h P_h} > Dk^2, \quad k\neq 0. \tag{83}$$

It is noted that this condition is not only sufficient but also necessary for instability, whereas in our previous works (Dai et al., 2005; Dai and Bai, 2008), the instability criterion ($G_h^{\xi} > Dk^2$) is only one of the sufficient conditions. It can be readily seen from (83) that the instability in coupling case depends not only on the creation G_h^{ξ} and diffusion Dk^2 of free volume but also on the strain hardening Q_h, strain rate hardening R_h, thermal diffusion κk^2, thermal softening P_h, free-volume softening F_h and free-volume creation ${G_h}^{\theta}$ due to temperature. Among them, Dk^2, κk^2, Q_h and R_h retard the perturbation growth, whereas ${G_h}^{\xi}$, ${G_h}^{\theta}$, P_h and F_h accelerate the instability. This is quite different from either the thermal softening or free-volume softening alone. As is expected, at short-wavelength limit, the system is again always stable due to the only negative root of spectral equation. For long wavelengths ($k\to 0$), the spectral equation becomes

$$\alpha^2 + a_3'\alpha + a_2' = 0, \tag{84}$$

where

$$a_3' = A\dot{\gamma}_h P_h - G_h^{\xi} + G_h^{\tau} F_h, \tag{85}$$

$$a_2' = -AG_h^{\xi}\dot{\gamma}_h P_h + AG_h^{\theta}\dot{\gamma}_h F_h. \tag{86}$$

Using the Routh–Hurwitz criterion again, the necessary and sufficient condition for instability is

$$a_3' < 0 \ \text{ or } \ a_2' < 0, \tag{87}$$

that is,

$$G_h^{\xi} > A\dot{\gamma}_h P_h + G_h^{\tau} F_h \ \text{ or } \ G_h^{\xi} > G_h^{\theta} F_h / P_h. \tag{88}$$

It is found that in the coupling softening, shear deformation is not always stable at $k \to 0$. This is consistent with that in the free-volume softening case, which implies that the instability resulting from coupled free-volume creation and thermal softening is dominated by free volume instead of temperature. If the thermal softening is dominant, then shear deformation must be always stable at $k \to 0$ due to the enhanced diffusion of momentum (inertia).

Also, according to the instability condition (83), the dynamic balance between the stabilizing and destabilizing effects determines a critical wavelength

$$l_c = 2\pi \left(\frac{2D\kappa R_h}{\sqrt{\Phi_1^2 + 4D\kappa R_h \Phi_2} - \Phi_1} \right)^{1/2} \tag{89}$$

with

$$\Phi_1 = (D+\kappa) Q_h - AD\tau_h P_h - \kappa R_h G_h^{\xi}, \tag{90}$$

$$\Phi_2 = Q_h G_h^{\xi} + A\tau_h F_h G_h^{\theta} - A\tau_h P_h G_h^{\xi}. \tag{91}$$

This is the coupling internal length scale, determining the growth or annihilation of perturbation. In the following, we still seek the internal time scale by examining the dominant instability mode in the coupling softening. By using the extremum condition (68) as well as the spectral Eq. (45), we obtain the dispersion equation (introducing $\Theta = {k_m}^2$):

$$N\Theta^2 + \Pi\Theta + O = 0, \tag{92}$$

where

$$N = 3D\kappa\left(Q_h/\rho + \nu\alpha_m\right), \tag{93}$$

$$\Pi = 2[\nu\kappa + D(\nu+\kappa)]\alpha_m^2 + 2\frac{(\kappa+D)Q_h - \kappa R_h G_h^{\xi} - AD\tau_h P_h}{\rho}\alpha_m - 2\frac{\kappa Q_h G_h^{\xi}}{\rho}, \tag{94}$$

$$O = (\nu+\kappa+D)\alpha_m^3 + \left[-(\nu+\kappa)G_h^{\xi} + \kappa F_h G_h^{\tau} + AD\dot{\gamma}_h P_h + \frac{Q_h}{\rho} - \frac{A\tau_h P_h}{\rho}\right]\alpha_m^2 + \frac{A\tau_h P_h G_h^{\xi} - Q_h G_h^{\xi} - A\tau_h F_h G_h^{\theta}}{\rho}\alpha_m. \tag{95}$$

Due to $\Theta = {k_m}^2 > 0$, Eq. (92) has at least one root that is larger than zero. According to the Routh–Hurwitz criterion and further considering the most dangerous status, i.e. $\kappa \to 0$ and $D \to 0$, we obtain that

$$0 < \alpha_m \le \frac{A\tau_h P_h - Q_h + G_h^{\xi} R_h + \sqrt{(A\tau_h P_h - Q_h - G_h^{\xi} R_h)^2 + 4A\tau_h G_h^{\theta} F_h R_h}}{2R_h}. \tag{96}$$

Thus, the internal time scale in the coupling softening instability is

$$t_c \sim \frac{2R_h}{A\tau_h P_h - Q_h + G_h^{\xi} R_h + \sqrt{(A\tau_h P_h - Q_h - G_h^{\xi} R_h)^2 + 4A\tau_h G_h^{\theta} F_h R_h}}. \tag{97}$$

According to the relative importance of the free-volume softening and thermal softening, the internal time scale given by (97) can be converted into the internal free volume or thermal time, respectively (Dai et al., 2005).

The internal length scale measures whether the instability occurs easily or with difficulty, while the internal time scale characterizes how fast does the instability initiate. More specifically, a decrease in the value of internal length and time scales indicates the hastening of initiation of the instability. Consequently we can calculate these scales in thermal softening, free-volume softening, and coupling softening, to determine who dominates the shear-banding instability in

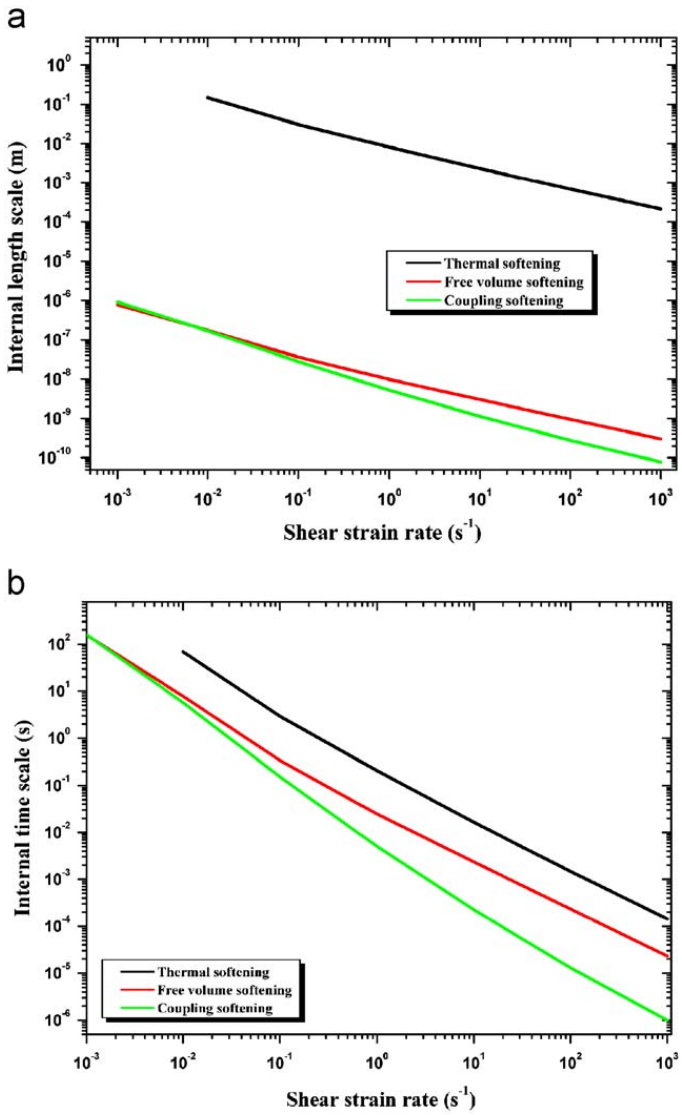

Fig. 7. Stability analysis of the homogeneous deformation: the dependence of shear strain rate on (a) internal length scale and (b) internal time scale.

BMGs; a typical range of strain rates from 10^{-3} to $10^{3}\,s^{-1}$ is considered here. The internal length and time scales are plotted against the applied strain rate in Fig. 7. It can be easily found from the figure that the internal scales of instability for the three cases decrease with increasing strain rate. This might be the main reason as to why the shear instability due to either thermal softening or free-volume creation is more probable at higher strain rates. This numerical result agrees well with the available experimental observations (Liu et al. 2005a, 2006). However, the situations in stability due to thermal softening and free-volume creation are quite different. The internal free-volume length and time scales are remarkably smaller than those in thermal softening, indicating that shear instability resulting from free-volume creation occurs easier and faster than thermal instability. At low strain rates, the thermal internal length and time scales are very large. This implies that thermal softening occurs with much difficulty at low strain rates. In particular, once the strain rate decreases to $10^{-3}\,s^{-1}$, the thermal softening becomes too weak to make shear instability any longer, because its instability criterion (60) is not satisfied. However, at this strain rate, the free-volume softening still appears. It is well known that shear-banding instability in BMGs occurs not only at high strain rate but also at quasi-static loading. So, it is very possible that shear banding or strain localization is set up by free-volume softening. This weak influence of thermal softening on shear instability at low strain rates results in the fact that the coupling shear instability behaviors are more like that due to free-volume creation. In such case, shear instability in BMGs is almost an isothermal process, during which the internal length scale is approximately tens of nanometers, and the internal time scale is roughly the inverse of strain rates. As the strain rate increases to dynamic range, such as $10^{3}\,s^{-1}$, the internal length scales due to both free-volume softening and coupling softening decrease to nanometers or sub-nanometers, while the thermal length scale is on a 10–100-μm scale. Also, the coupling softening with the internal time scale ~μs occurs much faster than the sole thermal softening with time scale ~ms. Therefore, under dynamic strain rate, the thermal softening is in favor of the shear instability originated from free-volume softening, leading to lower values of internal length and time scales in the coupling softening case.

Our theoretical analysis and numerical calculation of what is happening from homogeneous to inhomogeneous deformation in BMG systems obviously reveal that, *event under coupled thermo-mechanical deformation, the shear-banding instability in BMGs is free-volume-initiated, because the free-volume softening occurs much easier and faster than the thermal softening. At high strain rate, the thermal softening facilitates this shear-banding instability originated from free-volume creation*.

5. Coupled thermo-mechanical shear-band analysis

A reasoned description how free-volume motion results in macroscopic plastic shear flow was given by Spaepen (1977, 2006), Argon (1979), Falk and Langer (1998) and Johnson et al. (2002), where the dominant contributor to localization is generally believed to be a local change in the state of the glass, i.e. a local increase in free volume or evolution of structural order. Our results presented in previous sections discover this mechanism for shear-banding instability, allowing for the interaction of temperature and free volume. In this section we will examine such a physical picture in more quantitative detail.

A one-dimensional analysis of shear-band formation is now carried out by considering the planar layer again, as depicted in Fig. 1. Since shear bands are narrow zones of weaker (accidental internal clustering of free volume) material lying parallel to the shear direction x, we can envision the separation of deformation in this planar layer into a shear-band zone of volume fraction ϑ and remaining matrix zone covering a fraction $(1-\vartheta)$. The essential difference in these two zones is that the shear-band zone is of higher value of initiate free-volume concentration than that of the matrix. Without losing the generality, ϑ has a typical value of 10^{-6}. This means that the volume occupied by the shear band is much smaller than that of the matrix. We suppose further that the deformation in the band and matrix is approximately homogeneous. The subscripts b and m denote the zone inside the shear band and the remaining matrix. For the sake of compactness, we introduce $\imath = b$ or m. This geometric configuration was also considered by Argon (1979) and Steif et al. (1982) in their study of localization.

In the dimensionless variables defined previously, the governing equations, satisfied inside and outside the band, are written as

$$\frac{\partial\tilde{\tau}}{\partial\tilde{t}}\frac{1}{\tilde{\mu}}=\frac{\partial\gamma_\imath}{\partial\tilde{t}}-2\exp\left[E_A\left(1-\frac{1}{\tilde{\theta}_\imath}\right)\right]\exp\left(-\frac{1}{\xi_\imath}\right)\sinh\left(\frac{\tilde{\tau}}{\tilde{\theta}_\imath}\right), \tag{98}$$

$$\frac{\partial\xi_\imath}{\partial\tilde{t}}=\frac{1}{\chi}\exp\left[E_A\left(1-\frac{1}{\tilde{\theta}_\imath}\right)\right]\exp\left(-\frac{1}{\xi_\imath}\right)\left\{\frac{\tilde{\theta}_\imath}{\xi_\imath\tilde{\mu}\phi}\left[\cosh\left(\frac{\tilde{\tau}}{\tilde{\theta}_\imath}\right)-1\right]-\frac{1}{n_D}\right\}, \tag{99}$$

$$\rho C_{v\imath}\frac{\partial\tilde{\theta}_\imath}{\partial\tilde{t}}=\beta_{TQ}\frac{\tau_0}{\theta_0}\tilde{\tau}\frac{\partial\gamma_\imath^p}{\partial\tilde{t}}, \tag{100}$$

where $E_A=\Delta G^m/k_B\theta_0$. Note, in particular, that the introduction of Eq. (100) or temperature into the shear-band analysis is very different from the previous studies (Argon, 1979; Steif et al., 1982). In their works, the inhomogeneous deformation is isothermal, while here we treat it as a coupled *thermo-mechanical* process. It is of great interest to investigate whether a highly localized disturbance in free volume can lead to the shear-banding instability *with inclusion of temperature*. There is general consensus that a significant increase in strain rates and temperatures will emerge with the attendant shear instability; hence, the specific heat and the Taylor–Quinney coefficient in (100) are no longer constants. Here, the specific heat is defined by the Debye model as follows (Blakemore, 1973):

$$C_v(\tilde{\theta}_\imath\theta_0)=9Nk_B\left(\frac{\tilde{\theta}_\imath\theta_0}{\theta_D}\right)^3\int_0^{\theta_D/\tilde{\theta}_\imath\theta_0}\frac{x^4\exp(x)}{(\exp(x)-1)^2}\,\mathrm{d}x, \tag{101}$$

where N is the Avogadro number and θ_D the Debye temperature. The Taylor–Quinney coefficient is considered to be a function of irreversible part of the strain rate (Wang, 1992):

$$\beta_{TQ}\left(\frac{\partial\gamma_\imath^p}{t_0\partial\tilde{t}}\right)=\frac{1}{\pi}\,\mathrm{arctg}\left(\frac{1}{3}tg\frac{2\pi}{5}lg\left(\frac{\partial\gamma_\imath^p}{t_0\partial\tilde{t}}\right)\right)+\frac{1}{2}. \tag{102}$$

Note that $\lim_{\dot{\gamma}\to 0}\beta_{TQ}=0$ and $\lim_{\dot{\gamma}\to 0}\beta_{TQ}=1$ are satisfied.

The total strain rate $\dot{\gamma}$, as a prescribed constant, is equal to the volume-weighted average of the strain rate inside and outside the shear band; hence

$$\dot{\gamma}=(1-\vartheta)\dot{\gamma}_m+\vartheta\dot{\gamma}_b=\text{const.} \tag{103}$$

The initial conditions are as follows: $\theta_{\imath 0}=300\,\mathrm{K}$, $\xi_{m0}=0.05$, $\xi_b=\xi_{b0}$ and $\tau_\imath=0$. The initial free volume ξ_{b0} in the band zone is slightly higher than that in the matrix. This slight increase provides an initiate free-volume fluctuation, i.e. $\Delta\xi=\xi_b-\xi_m$, to weaken the material in the local zone, from which the shear band should be found to initiate. The governing equations (98)–(103) are simultaneously integrated numerically to determine the stress, free-volume, temperature in and outside the band zone as a function of applied macroscopic strain.

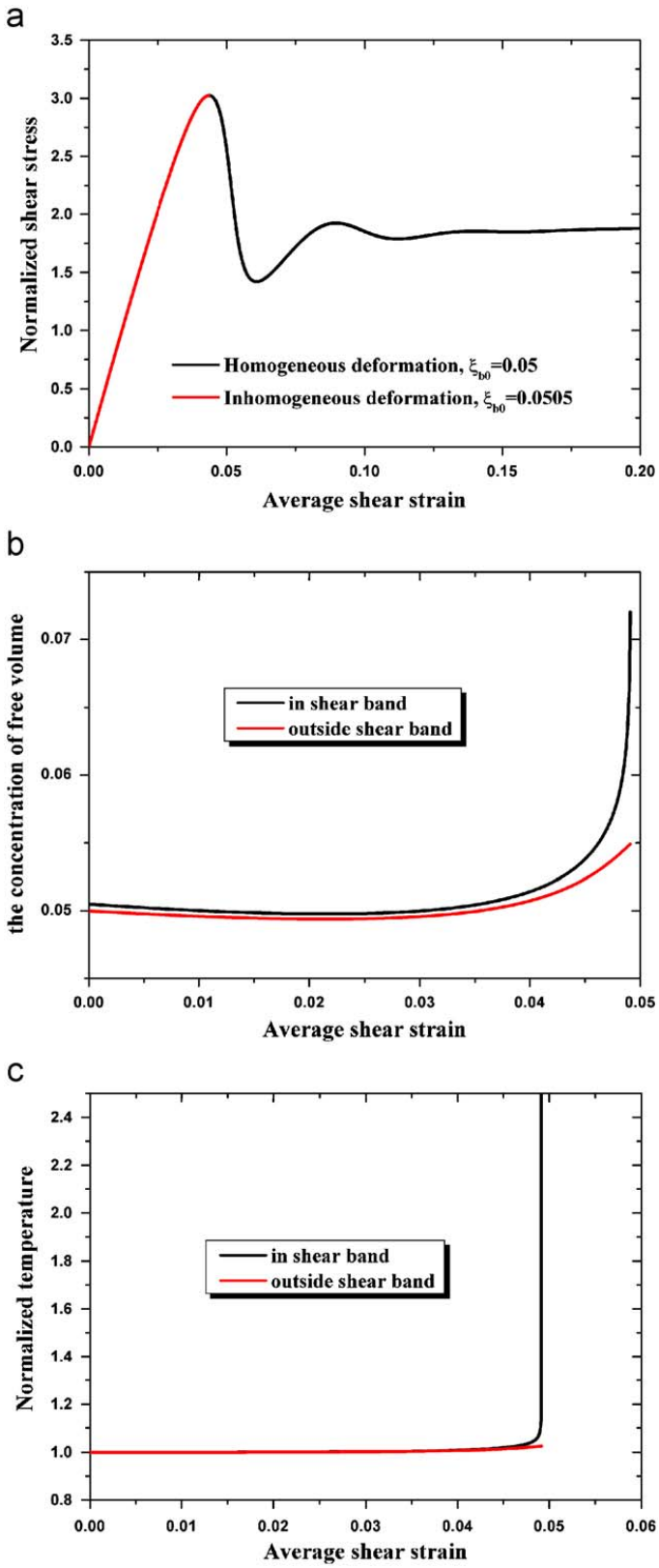

Fig. 8. The solution of inhomogeneous deformation at strain rate $\dot{\gamma} = 10^{-2}\,s^{-1}$: (a) normalized shear stress, (b) free-volume concentration, and (c) normalized temperature versus average shear strain. The shear stress inhomogeneous deformation with $\xi_{m0} = \xi_{b0} = 0.05$, for comparison, is also shown in (a).

For a typical set of physical parameters listed in Table 1 as well as $\dot{\gamma} = 10^{-2}\,s^{-1}$ and $\xi_{b0} = 0.0505$, the inhomogeneous solution including shear stress, free volume, and temperature as a function of applied strain is shown in Fig. 8. As seen in Fig. 8a, the inhomogeneous stress–strain curve exhibits an initial elastic deformation and immediate fracture without any

macroscopic plastic flow. This behavior is consistent with experimental observations under shear deformation (Liu et al., 2005a). However, if $\xi_{m0} = \xi_{b0} = 0.05$, the coupling homogeneous deformation, as shown in Fig. 2a, is recovered. In such case, a steady flow after an overshoot of stress is achieved, allowing for a significant plastic deformation (Lu et al., 2003). Fig. 8b shows the evolution of free volume, illustrating the significant increase of free-volume concentration in the shear band as the external shear strain increases, and the concomitant slight increase of free volume in the surrounding matrix. The evolution of temperature (Fig. 8c) also shows this trend. The result clearly reveals that the temperature increase can reach the glass transition temperature in the shear band even at a quasi-static strain rate (Yang et al., 2006a; Zhang et al., 2007), whereas the material outside almost keeps the initiate temperature at that moment. Since the initiate temperature throughout the sample is uniform, this local heating must result from the local creation of free volume in the band zone and is a second effect. We will clarify this point shortly.

The catastrophic character of strain localization or shear banding in metallic glasses, as shown in Fig. 9, is evident. Fig. 9a illustrates the remarkable acceleration of strain development in the shear band once a peak stress (Fig. 8a) has been reached, and the corresponding drop of strain rate in the matrix. The instantaneous temperature increase in the band should be ascribed to the occurrence of dynamic strain rate. In addition, the great increase of strain rate in the band results in the rapid increase of inner shear strain (Fig. 8b), giving rise to shear banding. During such a process, the viscosity (Fig. 10), defined in Eq. (26), in the band drastically decreases to a value of $\sim 10^{-5}$ poise, much smaller than that ($\sim 10^{11}$ poise) outside the band. It is well known that the initiation of shear-banding hinges strongly on the catastrophic drop in local viscosity. To ferret out the main reason for this material weakening, we calculated both the thermal instability index IN_θ and the free-volume instability index IN_ξ in the band during the deformation. A plot of the two instability indexes in the band as a function of the applied shear strain is shown in Fig. 11. The inset shows high magnification curve of the circled zone. Interestingly, we find that the sharp bend up in the curve of free-volume instability index is prior to that in the thermal instability. Moreover, the maximum of free-volume instability index is almost two times that of the thermal

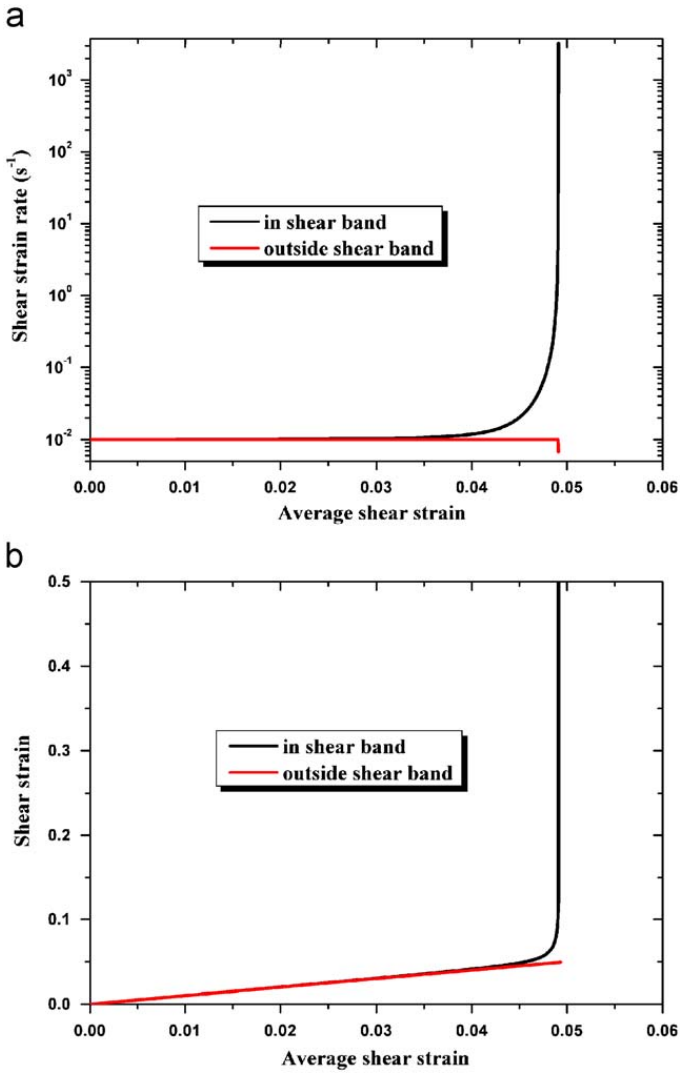

Fig. 9. The process of strain localization (or shear banding). A history of (a) strain rate and (b) strain is shown for both the forming shear banding and the surrounding matrix.

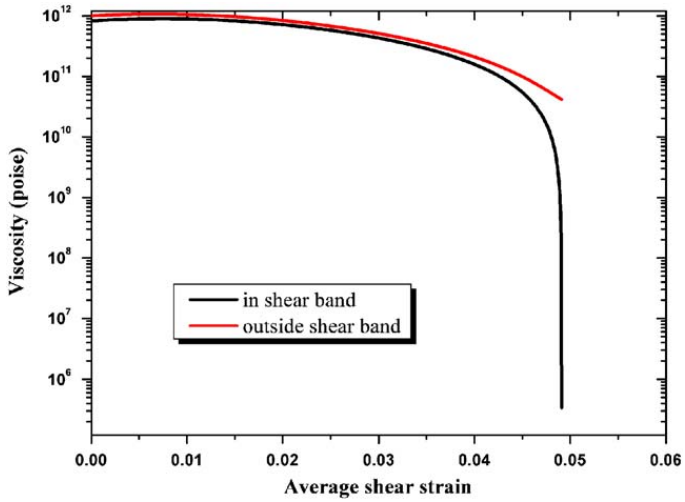

Fig. 10. Viscosity in and outside the band as function of the average shear strain.

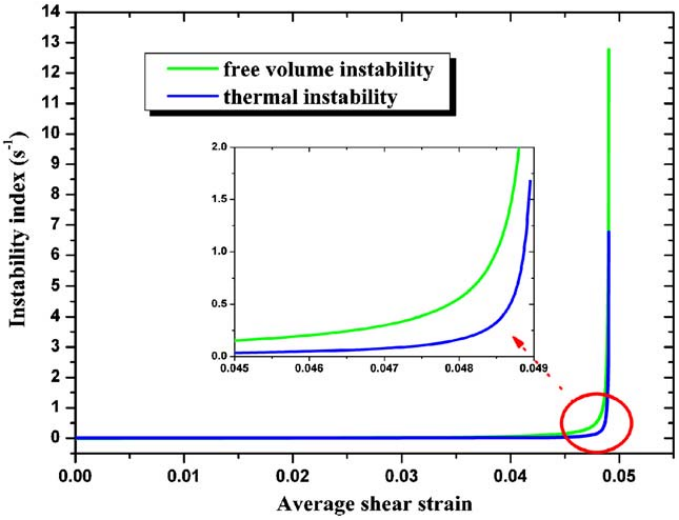

Fig. 11. The evolution of instability index in the shear band as the applied shear strain increases.

instability index. These results provide much clearer evidence that the local material softening or instability due to free-volume creation is *earlier and faster* than that due to temperature rise. This is well consistent with that given by the linear perturbation analysis. In addition, the temperature rise is the consequence of free-volume-induced shear localization, not its cause; this agrees well with MD simulations showing that heating occurs after the onset of localized shear (Bailey et al., 2006). Our results provide a powerful theoretical expatiation on the puzzle about temperature rise at shear bands and thickness of shear bands in metallic glasses (Lewandowski and Greer, 2006; Zhang and Greer, 2006a). The local free-volume creation, as the origin of shear localization, controls shear-band thickness (Jiang et al., 2009a), while local temperature rise, as a secondary effect, strongly depends on the development of this shear localization (Zhang et al., 2007, 2008).

Furthermore, the influence of free-volume fluctuation on shear-banding instability is examined. The result that the shear strain in the shear band is plotted against the total shear strain under different fluctuation of free volume is shown in Fig. 12. From this graph, it is obviously seen that the critical strain at which the strain localization occurs decreases with increase in free-volume fluctuation. The trend shows that the more heterogeneous a material is, the more *easily or earlier* the shear localization occurs. For comparison, we calculate the case without free-volume fluctuation, i.e. $\Delta\xi = 0$, corresponding to the straight line: $\gamma_b = \gamma$. In such case, the shear instability does not initiate, whereas homogeneous deformation occurs. Our result is consistent with the fundamental concept underlying enhancement of ductility and toughening proposed by Liu et al. (2007) and Hofmann et al. (2008). That is introducing of 'soft' elastic/plastic inhomogeneities in a metallic glass matrix to initiate local shear banding around or in the inhomogeneity. Compared to the matrix, these inhomogeneous phases are softer zones where or around where there are much more thermally unstable atomic-scale open volumes, i.e. free volume, serving as the nucleation sites for the shear bands. Consequently, numerous shear-banding nuclei are formed concurrently in these locally free-volume-perturbed regions and evolve into multiple

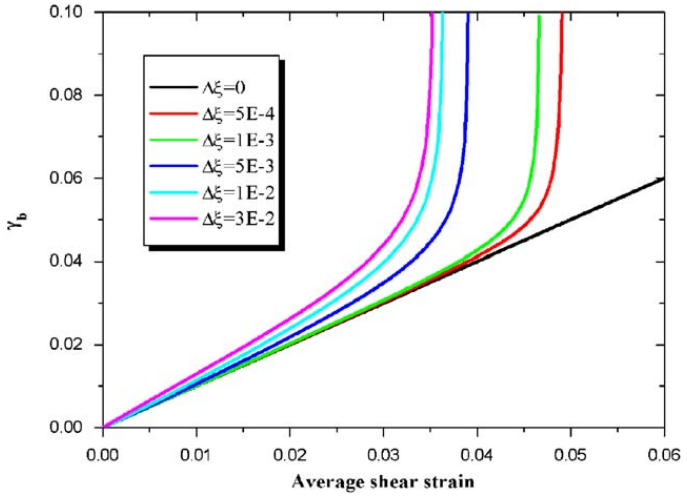

Fig. 12. The effect of free-volume perturbation on strain localization.

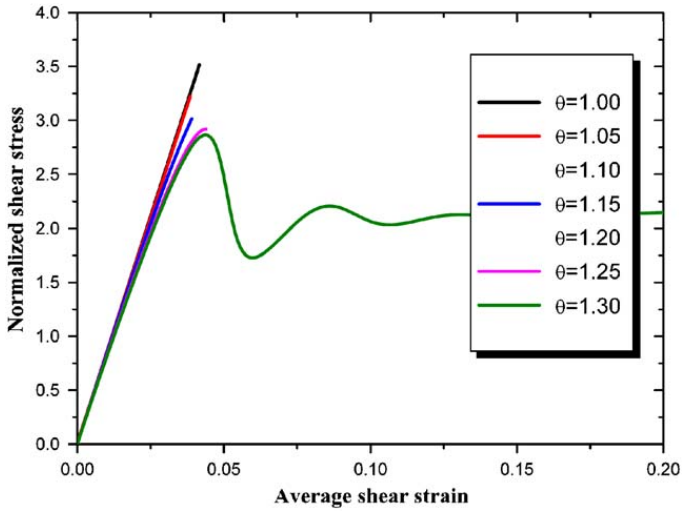

Fig. 13. Effect of temperature on the shear stress–strain behavior at a strain rate of $10^{-2}\,s^{-1}$.

shear bands upon loading. These shear bands can be interrupted by each other at their intersection sites or by a relatively hard matrix; thus, their propagation is blocked. This blocking behavior prevents the BMG from fracturing quickly along a single shear band (Liu et al., 2005b). In other words, the formation of intersecting shear bands can compensate the softening induced by their formation and then enhance the plasticity of BMGs. For example, based on the Poisson's ratio criterion (Lewandowski et al., 2005), Liu et al. (2007) created the super plastic bulk metallic glasses composed of hard regions surrounded by softer regions. This unique microstructure enables the glasses to undergo true strain of more than 160%. Very recently, Hofmann et al. (2008), through designed compositional changes, obtained the composite of the 'soft' body-centred cubic (b.c.c.) dendritic phase and glass matrix with room-temperature tensile ductility exceeding 10% and K_{IC} up to $\sim$170 MPa $m^{1/2}$. These 'soft' regions or crystalline inclusions lead to much acute fluctuation in local free volume, facilitating the concurrence of shear-banding instability.

Finally, the present model can also predict the transition from inhomogeneous (shear-band localization) to homogeneous deformation at elevated temperature or decreased strain rate. Fig. 13 shows the shear stress–strain behaviors at a strain rate of $10^{-2}\,s^{-1}$ for normalized temperature in the range of 1.0–1.3. The stress–strain curves at lower temperature have a linear slope until failure and no plastic post-yielding was evident. After reaching the peak stress, the stress drops to its zero value immediately, typical of 'shear-band localization' failure. However, increasing temperature to 1.30 leads to a transition from inhomogeneous deformation to homogeneous flow. Fig. 14 illustrates the shear stress–stain curves at a normalized room temperature of 1.0 for strain rate ranging from 10^{-4} to $10^{1}\,s^{-1}$. It is found that shear-localized failure characterizes the deformation mode at higher strain rates in the range of 10^{-2}–$10^{1}\,s^{-1}$. When the strain rate decreases to the 10^{-3}–$10^{-4}\,s^{-1}$ range, the shear–strain curves display obvious homogeneous flow after yielding. It is also clear that increase in strain rate leads to a transition from homogenous flow to inhomogeneous deformation. Therefore, the effect on the deformation mode due to a decrease in strain rate is similar to that due to increase in ambient temperature. Our theoretical results are in agreement with the experimental observations by Lu et al. (2003).

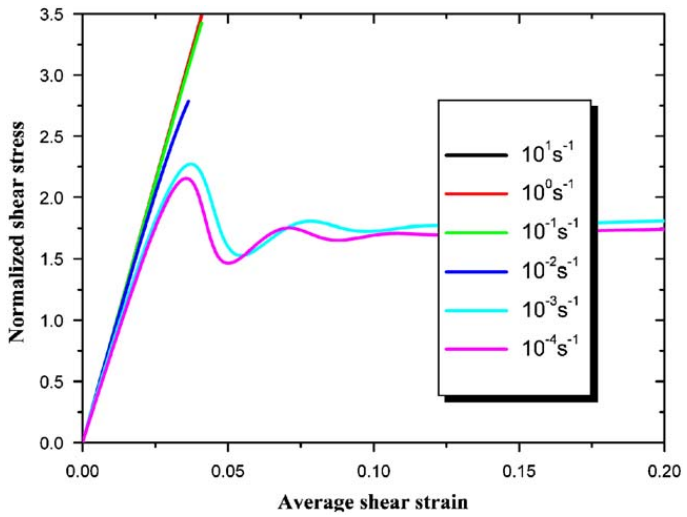

Fig. 14. Effect of strain rate on the shear stress–strain behavior at a normalized ambient temperature of 1.0.

6. Effect of shear-induced dilatation on shear stability

It has long been known that disordered materials experience dilatation due to plastic deformation (Reynolds, 1885; Taylor, 1948). So for metallic glasses, it has been widely expected that the hydrostatic stress or the normal stress acting on the shear plane will play a role on (localized) plastic flow (Flores and Dauskardt, 2001; Schuh and Lund, 2003; Zhang et al., 2003; Zhao and Li, 2008; Jiang et al., 2008, 2009b). In what follows, we will briefly discuss the effect of the shear-induced dilatation on shear-banding instability in BMGs by extension of the perturbation analysis. For simplicity, we still consider the planar layer, as shown in Fig. 1, but taking into account the dilatation of sample. The upper and lower surfaces are loaded with a constant average shear strain rate $\dot{\gamma}$. As the shear stress creates more free volume, the sample dilates. When the dilatation is non-uniform across the layer, geometric constraint will induce normal stress in the x and z directions. The normal stresses are assumed equal in both directions, i.e., $\sigma_{xx}=\sigma_{zz}=\sigma(y,t)$. Compared to the x and z directions, the material dilates with very slight constrain along the y direction. Therefore, we can reasonably assume that $\sigma_{xx}=\sigma_{zz}\gg\sigma_{yy}$. Simulation on shear deformation of metallic glass also shows this trend (Ogata et al., 2006). Note that even there is a geometric constrain in the y direction, the normal stress σ_y can be assumed to be zero so long as $(\tau/\mu)\ll 1$ is satisfied (Shawki and Clifton, 1989). For simplicity, we therefore take $\sigma_y\to 0$ under the small deformation conditions. In fact, the identical treatment of setting $\sigma_y\to 0$ was adopted in the work of Huang et al. (2002). Under such a stress state, we can define an effective stress σ_e as

$$\sigma_e = mI_1 + \sqrt{J_2}, \tag{104}$$

where m is the pressure sensitivity index, similar to the friction coefficient and measuring the ratio of deviatotic to hydrostatic stress, I_1 is the fist invariant of the stress tensor and $J_2=\mathbf{ss}/2$ with $\mathbf{s}$ as the deviatoric stress tensor. Relation (104) is from the Drucker–Prager yield criterion in which the hydrostatic pressure is considered contributing a part to the plastic flow. In this case, the momentum balance still satisfies Eq. (6) in Section 2. The total shear strain becomes

$$\dot{\gamma} = \frac{1}{\mu}\frac{\mathrm{d}\tau}{\mathrm{d}t} + f_l(\xi,\theta,\sigma_e)\frac{\tau}{\sqrt{J_2}}, \tag{105}$$

where f_l is the flow rate depending on the concentration of free volume ξ, the temperature θ and the effective stress σ_e, which can be generalized from Spaepen (1977) by $\tau=\sigma_e$, with the following form:

$$f_l(\xi,\theta,\sigma_e) = 2f\exp\left(-\frac{\Delta G^m}{k_B\theta}\right)\exp\left(-\frac{1}{\xi}\right)\sinh\left(\frac{\sigma_e\Omega}{2k_B\theta}\right). \tag{106}$$

Further assume that, by the geometric constraint, the normal strains are equal in the x and z directions, i.e., $\varepsilon_{xx}=\varepsilon_{zz}=\varepsilon(y,t)$. Also, the normal strain consists of the elastic strain and the plastic strain, as follows:

$$\dot{\varepsilon} = \frac{1-2\nu}{2\mu}\frac{\mathrm{d}\sigma}{\mathrm{d}t} + f_l(\xi,\theta,\sigma_e)\frac{\sigma}{6\sqrt{J_2}}. \tag{107}$$

In addition, we introduce a dilatancy factor following Rudnicki and Rice (1975) as follows:

$$\ell = \frac{\mathrm{d}\varepsilon}{\mathrm{d}\gamma} > 0. \tag{108}$$

This parameter indicates the ratio of the normal to shear strain, which is taken to be fixed during deformation for simplicity.

Assuming that the temperature and the concentration of free volume are uniform along the x and z directions but vary along the y direction, their evolution equations are, respectively,

$$\frac{\partial\theta}{\partial t}=\kappa\frac{\partial^2\theta}{\partial y^2}+A\sigma_e\frac{\partial\varepsilon_e}{\partial t} \tag{109}$$

and

$$\frac{\partial\xi}{\partial t}=D\frac{\partial^2\xi}{\partial y^2}+G(\xi,\theta,\sigma_e). \tag{110}$$

The two equations state that, not only the shear stress but also the hydrostatic stress originated from volume dilatation can drive the production of free volume as well as temperature.

Again, we perform a linear stability analysis by imposing a small perturbation $(\delta\tau,\delta\gamma,\delta\theta,\delta\xi,\delta\sigma,\delta\varepsilon)=(\tau_*,\gamma_*,\theta_*,\xi_*,\sigma_*,\varepsilon_*)\exp(\alpha t+iky)$ on the smoothly developing homogeneous state $(\tau_h,\gamma_h,\theta_h,\xi_h,\sigma_h,\varepsilon_h)$. As handled in Section 4, we can obtain the instability criterion for the current case,

$$G_h^{\xi}(\xi,\theta,\sigma_{eh})+\frac{A\sigma_{eh}F_hG_\theta-\kappa(1-\ell)Q_hk^2}{\kappa R_hk^2+(1-\ell)Q_h-A\sigma_{eh}P_h}>Dk^2. \tag{111}$$

It is found that this criterion is similar to that (83) in the coupling softening, except that τ_h and Q_h are replaced by σ_{eh} and $(1-\ell)Q_h$, respectively. Obviously, increasing dilatancy factor ℓ reduces the strain hardening from Q_h to $(1-\ell)Q_h$, facilitating

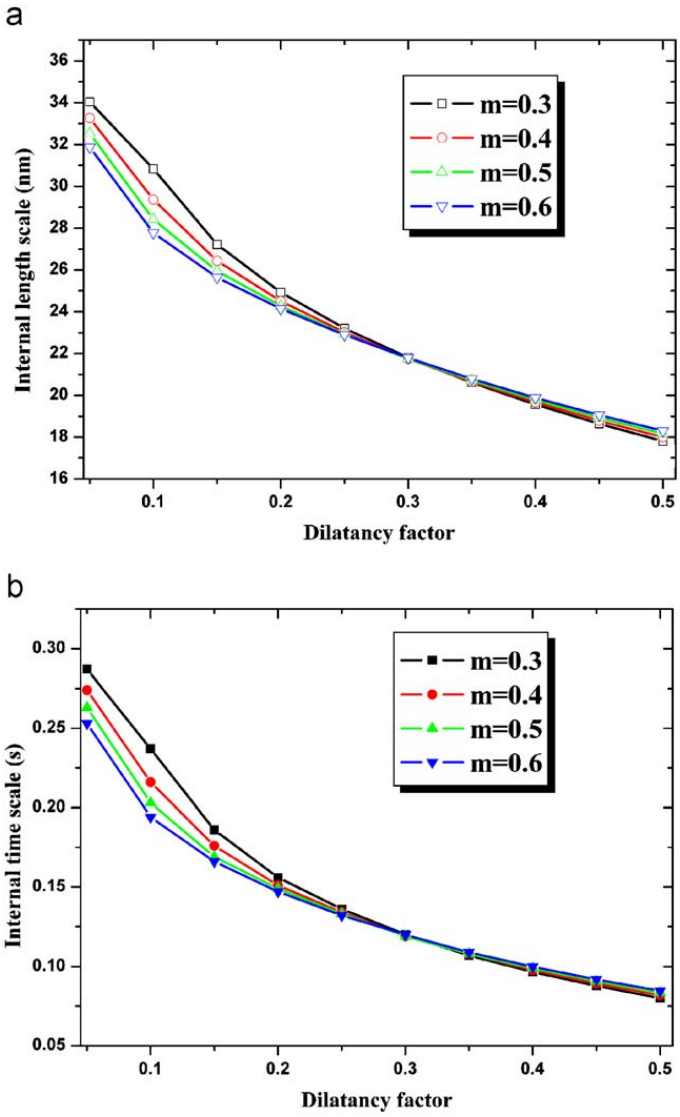

Fig. 15. Internal (a) length scale and (b) time scale vs. dilatancy factor with various pressure insensitivity indexes.

the shear instability. However, whether σ_e accelerates the instability or not depends on the dilatability or ℓ (*vide post*). Similar to foregoing analysis, the internal length and time scales are also obtained only by making the identifications $\tau_h = \sigma_{eh}$ and $Q_h = (1-\ell)Q_h$ in Eqs. (89) and (97).

As pointed out previously, the internal length scale measures whether the instability occurs easily or with difficulty, while the internal time scale characterizes how fast does the instability initiate. Thus, we can calculate these internal scales to examine the effects of the pressure sensitivity index m and dilatancy factor ℓ on shear instability. For the Zr-based BMGs, the pressure sensitivity index m_{mc} in the Mohr-Coulomb criterion is about 0.2–0.4 range (Lund and Schun, 2003). The pressure sensitivity index m in the Drucker–Prager criterion is related to m_{mc} by Chen and Han (1988) $m = \sqrt{3}\sin(\arctan m_{mc})$. Therefore, m is estimated to be 0.3–0.6. A representative range of ℓ is inferred as 0.2–0.4 for pressure-sensitive dilatant materials by Rudnicki and Rice (1975). Here, we arbitrarily choose $\ell = 0.05-0.5$ for metallic glasses. Fig. 15 shows the internal length and time scales vs. the dilatancy factor with various pressure sensitivity indices. It can be found that the internal scales for shear instability decrease with increase in dilatancy factor for any fixed m. This means that the shear-induced dilatation strain makes the shear-banding instability easier and faster. However, the effect of hydrostatic pressure on shear instability is more complex. It is noted from this picture that these curves have a point of crossing at $\ell_c \approx 0.3$. When $\ell < l_c$, these scales decrease with increase in m, indicating that the tensile hydrostatic pressure further accelerates shear instability. The reason is that, in this case, σ_e is always greater than τ and monotonically increases with increasing m. However, in the opposite case, i.e., when the dilatation is greater than the critical point, the dilatation-induced hydrostatic stress can retard slightly the shear instability, because the effective stress is always smaller than the shear stress. Thus we can conclude that the tensile hydrostatic stress can play a positive or negative role on shear instability, which depends on the intrinsic dilatability of various BMGs. Our previous analysis indicates that, in a real flow event, the shear-induced dilatation strain is about 0.1 of shear yield strain for a number of metallic glasses (Jiang and Dai, 2007). Thus, for such dilatability ($\ell = 0.1$), the tensile hydrostatic stress further helps in shear instability according to the present results (Fig. 15), which is consistent with the experimental observations by Flores and Dauskardt (2001). Our later work will focus on the relationship between the pressure sensitivity index and the dilatancy factor, which is important to understand the pressure-dependent deformation and fracture behaviors of metallic glasses.

7. Conclusion

This paper presents a theoretical description for a bulk metallic glass undergoing a one-dimensional simple shear to understand whether the shear-banding instability of BMGs is essentially free-volume-dominant or adiabatic shear-induced. The homogeneous deformation before instability and subsequent linear perturbation analysis clearly reveal the totally different mechanism for shear-banding instability due to free-volume softening and classical thermal softening. Furthermore, a coupled thermo-mechanical shear-band analysis is performed to capture the free-volume-initiated shear-banding instability phenomenon. Our results suggest a clear physical picture of shear-banding instability upon loading a bulk metal glass. Strains first respond elastically to the applied stress, until the stress level reaches the yielding point, where it can activate inelastic/plastic flow in a locally free-volume perturbed region. Owing to the perturbation growth, there is a mismatch in strain rate between the perturbed (shear band) and unperturbed (matrix) zone. The strain rate in the shear band significantly grows as the applied macroscopic strain increases, and the concomitant decrease in shear strain rate in the surrounding matrix. The increased strain rate accumulation in the perturbed region is accompanied by strain softening, which further exacerbates the rate mismatch at lightning speed. The strain in the band therefore becomes very large and strain localization or shear band appears. During the process of strain localization, an instantaneous local temperature increase occurs due to the achievement of dynamic plastic strain rate in the shear-band region. This temperature increase in turn speeds up the net creation of free volume and facilitates shear-banding instability originated from local free-volume perturbation. The shear-induced dilatation facilitates such shear-banding instability in BMGs.

The present work has analyzed the shear-banding instability of BMGs, clearly revealing that it is free volume by origin. This is an important step in understanding the shear-band behavior in BMGs. The coupled thermo-mechanical post-instability process deserves to be studied in our later work. Our study also provides useful theoretical guidance to improving the ductility and reliability of BMGs.

Acknowledgements

This work has been supported by the Natural Science Foundation of China (Grants nos. 10725211 and 10721202), the National Basic Research Program of China (Grant no. 2009CB724401) and the Key Project of Chinese Academy of Sciences (Nos. KJCX2-YW-M04 and KJCX-SW-L08). We are highly grateful to two anonymous reviewers for their helpful comments, which have improved our manuscript significantly.

References

Argon, A.S., 1979. Plastic deformation in metallic glasses. Acta Metall. 27, 47–58.
Ashby, M.F., Greer, A.L., 2006. Metallic glasses as structural materials. Scr. Mater. 54, 321–326.

Bai, Y.L., 1982. Thermo-plastic instability in simple shear. J. Mech. Phys. Solids 30, 195–207.
Bai, Y.L., Dodd, B., 1992. Adiabatic Shear Localization. Pergamon Press, Oxford.
Bailey, N.P., Schiøtz, J., Jacobsen, K.W., 2006. Atomistic simulation study of the shear-band deformation mechanism in Mg–Cu metallic glasses. Phys. Rev. B 73, 064108.
Bengus, V.Z., Tabachnikova, E.D., Shumilin, S.E., Golovin, Y.L., Makarov, M.V., Miskuf, J., Csach, K., Ocelik, V., 1993. Some peculiarities of ductile shear failure of amorphous alloy ribbons. Int. J. Rapid Solid 8, 21–31.
Blakemore, J.S., 1973. Solid State Physics, second ed. W.B. Saunders Co., Philadelphia.
Chen, H.S., 1974. Thermodynamic considerations on the formation and stability of metallic glasses. Acta Mater. 22 (12), 1505–1511.
Chen, L.Y., Fu, Z.D., Zhang, G.Q., Hao, X.P., Jiang, Q.K., Wang, X.D., Cao, Q.P., Franz, H., Liu, Y.G., Xie, H.S., Zhang, S.L., Wang, B.Y., Zeng, Y.W., Jiang, J.Z., 2008. New class of plastic bulk metallic glass. Phys. Rev. Lett. 100, 075501.
Chen, W.F., Han, D.J., 1988. Plasticity of Structural Engineers. Springer, Berlin.
Chichili, D.R., Ramesh, K.T., Hemker, K.J., 2004. Adiabatic shear localization in α-titanium: experiments, modeling and microstructural evolution. J. Mech. Phys. Solids 52, 1889–1909.
Clifton, R.J., Duffy, J., Hartley, K.A., Shawki, T.G., 1984. On critical condition for shear band formation at high strain rates. Scr. Mater. 18, 443–448.
Conner, R.D., Dandliker, R.B., Scruggs, V., Johnson, W.L., 2000. Dynamic deformation behavior of tungsten-fiber/metallic-glass matrix composites. Int. J. Impact Eng. 24, 435–444.
Dai, L.H., Bai, Y.L., 2008. Basic mechanical behaviors and mechanics of shear banding in BMGs. Int. J. Impact Eng. 35, 704–716.
Dai, L.H., Liu, L.F., Bai, Y.L., 2004. Formation of adiabatic shear band in metal matrix composites. Int. J. Solids Struct. 41, 5979–5993.
Dai, L.H., Yan, M., Liu, L.F., Bai, Y.L., 2005. Adiabatic shear banding instability in bulk metallic glasses. Appl. Phys. Lett. 87, 141916.
Das, J., Tang, M.B., Kim, K.B., Theissmann, R., Baier, F., Wang, W.H., Eckert, J., 2005. "Work-hardenable" ductile bulk metallic glass. Phys. Rev. Lett. 94, 205501.
Donovan, P.E., Stobbs, W.M., 1981. The structure of shear bands in metallic glasses. Acta Metall. 29, 1419–1436.
Drehman, A.L., Greer, A.L., Turnbull, D., 1982. Bulk formation of a metallic glass: $Pd_{40}Ni_{40}P_{20}$. Appl. Phys. Lett. 41, 716–717.
Eckert, J., Das, J., Pauly, S., Duhamel, C., 2007. Mechanical properties of bulk metallic glasses and composites. J. Mater. Res. 22, 285–301.
Falk, M.L., Langer, J.S., 1998. Dynamics of viscoplastic deformation in amorphous solids. Phys. Rev. E 57, 7192–7205.
Flores, K.M., Dauskardt, R.H., 2001. Mean stress effects on flow localization and failure in a bulk metallic glass. Acta Mater. 49, 2527–2537.
Gao, Y.F., Yang, B., Nieh, T.G., 2007. Thermomechanical instability analysis of inhomogeneous deformation in amorphous alloys. Acta Mater. 55, 2319–2327.
Grady, D.E., 1992. Properties of an adiabatic shear-band process zone. J. Mech. Phys. Solids 40, 1197–1215.
Greer, A.L., 1995. Metallic glasses. Science 267, 1947–1953.
Grimberg, A., Baur, H., Bochsler, P., Buhler, F., Burnett, D.S., Hays, C.C., Heber, V.S., Jurewicz, A.J.G., Wieler, R., 2006. Solar wind neon from genesis: implications for the lunar noble gas record. Science 314, 1133–1135.
Hays, C.C., Kim, C.P., Johnson, W.L., 2000. Microstructure controlled shear band pattern formation and enhanced plasticity of bulk metallic glasses containing in situ formed ductile phase dendrite dispersions. Phys. Rev. Lett. 84, 2901–2904.
Hofmann, D.C., Suh, J.Y., Wiest, A., Duan, G., Lind, M.L., Demetriou, M.D., Johnson, W.L., 2008. Designing metallic glass matrix composites with high toughness and tensile ductility. Nature 451, 1085–1089.
Huang, R., Suo, Z., Prevost, J.H., Nix, W.D., 2002. Inhomogeneous deformation in metallic glasses. J. Mech. Phys. Solids 50, 1011–1027.
Hufnagel, T.C., El-Deiry, P., Vinci, R.P., 2000. Development of shear band structure during deformation of a $Zr_{57}Ti_5Cu_{20}Ni_8Al_{10}$ bulk metallic glass. Scr. Mater. 43, 1071–1075.
Hufnagel, T.C., Jiao, T., Li, Y., Xing, L.-Q., Ramesh, K.T., 2002. Deformation and failure of $Zr_{57}Ti_5Cu_{20}Ni_8Al_{10}$ bulk metallic glass under quasi-static and dynamic compression. J. Mater. Res. 17, 1441–1445.
Inoue, A., 2000. Stabilization of metallic supercooled liquid and bulk amorphous alloys. Acta Mater. 48, 279–306.
Inoue, A., Zhang, T., Masumoto, T., 1989. Al–La–Ni amorphous alloys with a wide supercooled liquid region. Mater. Trans. JIM 30, 965–972.
Jiang, M.Q., Dai, L.H., 2007. Intrinsic correlation between fragility and bulk modulus in metallic glasses. Phys. Rev. B 76, 054204.
Jiang, M.Q., Ling, Z., Meng, J.X., Dai, L.H., 2008. Energy dissipation in fracture of bulk metallic glasses via inherent competition between local softening and quasi-cleavage. Phil. Mag. 88, 407–426.
Jiang, M.Q., Wang, W.H., Dai, L.H., 2009a. Prediction of shear-band thickness in metallic glass. Scr. Mater. 60, 1004–1007.
Jiang, M.Q., Jiang, S.Y., Dai, L.H., 2009b. Inherent shear-dilatation coexistence in metallic glass. Chin. Phys. Lett. 26, 016103.
Johnson, W.L., 1999. Bulk glass-forming metallic alloys: science and technology. MRS Bull. 24, 42–56.
Johnson, W.L., Lu, J., Demetriou, M.D., 2002. Deformation and flow in bulk metallic glasses and deeply undercooled glass forming liquids—a self consistent dynamic free volume model. Intermetallics 10, 1039–1046.
Johnson, W.L., Samwer, K., 2005. A universal criterion for plastic yielding of metallic glasses with a $(T/T_g)^{2/3}$ temperature dependence. Phys. Rev. Lett. 95, 195501.
Klement, W., Willens, R.H., Duwez, P., 1960. Non-crystalline structure in solidified gold–silicon alloys. Nature 187, 869–870.
Kumar, G., Tang, H.X., Schroers, J., 2009. Nanomoulding with amorphous metals. Nature 457, 868–872.
Leamy, H.J., Chen, H.S., Wang, T.T., 1972. Plastic flow and fracture of metallic glass. Metall. Trans. 3, 699–708.
Lewandowski, J.J., Greer, A.L., 2006. Temperature rise at shear bands in metallic glasses. Nat. Mater. 5, 15–18.
Lewandowski, J.J., Wang, W.H., Greer, A.L., 2005. Intrinsic plasticity or brittleness of metallic glasses. Phil. Mag. Lett. 85, 77–87.
Li, J., Spaepen, F., Hufnagel, T.C., 2002. Nanometer-scale defects in shear bands in a metallic glass. Phil. Mag. A 82, 2623–2630.
Liu, C.T., Heatherly, L., Easton, D.S., Carmichael, C.A., Wright, J.L., Schneibel, J.H., Yoo, M.H., Chen, C.H., Inoue, A., 1998. Test environments and mechanical properties of Zr-base bulk amorphous alloys. Metall. Mater. Trans. A 29, 1811–1820.
Liu, L.F., Dai, L.H., Bai, Y.L., Wei, B.C., 2005a. Initiation and propagation of shear bands in Zr-based bulk metallic glass under quasi-static and dynamic shear loadings. J. Non-Cryst. Solids 351, 3259–3270.
Liu, L.F., Dai, L.H., Bai, Y.L., Wei, B.C., Eckert, J., 2005b. Behavior of multiple shear bands in Zr-based bulk metallic glass. Mater. Chem. Phys. 93, 174–177.
Liu, L.F., Dai, L.H., Bai, Y.L., Wei, B.C., Eckert, J., 2006. Characterization of rate-dependent shear behavior of Zr-based bulk metallic glass using shear-punching testing. J. Mater. Res. 21 (1), 153–160.
Liu, Y.H., Wang, G., Wang, R.J., Zhao, D.Q., Pan, M.X., Wang, W.H., 2007. Super bulk metallic glasses at room temperature. Science 315, 1385–1388.
Lu, J., Ravichandran, G., Johnson, W.L., 2003. Deformation behavior of the Zr41.2Ti13.8Cu12.5Ni10Be22.5 bulk metallic glass over a wide range of strain rates and temperatures. Acta Mater. 51, 3429–3443.
Lund, A.C., Schuh, C.A., 2003. Yield surface of a simulated metallic glass. Acta Mater. 51, 5399–5411.
Meyers, M.A., 1994. Dynamic Behavior of Materials. Wiley, New York.
Molinari, A., 1997. Collective behavior and spacing of adiabatic shear bands. J. Mech. Phys. Solids 45 (9), 1551–1575.
Moura-Ramos, J.J., Correia, N.T., 2001. The Deborah number, relaxation phenomenon and thermally simulated currents. Phys. Chem. Chem. Phys. 3, 5575–5578.
Ogata, S., Shimizu, F., Li, J., Wakeda, M., Shibutani, Y., 2006. Atomistic simulation of shear localization in Cu–Zr bulk metallic glass. Intermetallics 14, 1033–1037.
Pampillo, C.A., 1975. Flow and fracture in amorphous alloys. J. Mater. Sci. 10, 1194–1227.
Peker, A., Johnson, W.L., 1993. A highly processable metallic glass: Zr–Ti–Cu–Ni–Be. Appl. Phys. Lett. 63, 2342–2344.
Reiner, M., 1964. The Deborah number. Phys. Today 17, 62.
Reynolds, O., 1885. On the dilatancy of media composed of rigid particles in contact, with experimental illustrations. Phil. Mag. 20, 469–481.

Rudnicki, J.W., Rice, J.R., 1975. Conditions for the localization of deformation in pressure-sensitive dilatant materials. J. Mech. Phys. Solids 23, 371–394.
Sanchez, D.A., 1968. Ordinary Differential Equations and Stability Theory. Freeman, San Francisco.
Schroers, J., Johnson, W.L., 2004. Ductile bulk metallic glass. Phys. Rev. Lett. 93, 255506.
Schuh, C.A., Hufnagel, T.C., Ramamurty, U., 2007. Mechanical behavior of amorphous alloys. Acta Mater. 55, 4067–4109.
Schuh, C.A., Lund, A.C., 2003. Atomistic basis for the plastic yield criterion of metallic glass. Nat. Mater. 2, 449–452.
Shawki, T.G., Clifton, R.J., 1989. Shear band formation in thermal viscoplastic materials. Mech. Mater. 8, 13–43.
Spaepen, F., 1977. A microscopic mechanism for steady state inhomogeneous flow in metallic glasses. Acta Metall. 25, 407–415.
Spaepen, F., 2006. Must shear bands be hot? Nat. Mater. 5, 7–8.
Steif, P.S., Spaepen, F., Hutchinson, J.W., 1982. Strain localization in amorphous metals. Acta Metall. 30, 447–455.
Taub, A.I., Spaepen, F., 1980. The kinetic of structural relaxation of a metallic glass. Acta Metall. 28, 1781–1788.
Taylor, D.W., 1948. Fundamentals of Soil Mechanics. Wiley, New York.
Thamburaja, P., Ekambaram, R., 2007. Coupled thermo-mechanical modelling of bulk-metallic glasses: theory, finite-element simulations and experimental verification. J. Mech. Phys. Solids 55, 1236–1273.
Turnbull, D., Cech, R.E., 1950. Microscopic observation of the solidification of small metal droplets. J. Appl. Phys. 21, 804–810.
Vaks, V.G., 1991. Possible mechanism for formation of localized shear bands in amorphous alloys. Phys. Lett. A 159, 174–178.
Wang, L.L., 1992. Advances in Impact Dynamics. University of Science and Technology of China Press, Hefei.
Wang, W.H., 2006. Correlations between elastic moduli and properties in bulk metallic glasses. J. Appl. Phys. 99, 093506.
Wang, W.H., Dong, C., Shek, C.H., 2004. Bulk metallic glasses. Mater. Sci. Eng. R 44, 45–89.
Wright, T.M., 2002. The Physics and Mathematics of Adiabatic Shear Bands. Cambridge University Press, Cambridge.
Wright, W.J., Hufangel, T.C., Nix, W.D., 2003. Free volume coalescence and void formation in shear bands in metallic glass. J. Appl. Phys. 93, 1432–1437.
Wright, W.J., Schwarz, R.B., Nix, W.D., 2001. Localized heating during serrated plastic flow in bulk metallic glasses. Mater. Sci. Eng. A 319–321, 229–232.
Yang, B., Liu, C.T., Nieh, T.G., Morrison, M.L., Liaw, P.K., Buchanan, R.A., 2006a. Localized heating and fracture criterion for bulk metallic glasses. J. Mater. Res. 21, 915–922.
Yang, B., Morrison, M.L., Liaw, P.K., Buchanan, R.A., Wang, G.Y., Liu, C.T., Denda, M., 2005. Dynamic evolution of nanoscale shear bands in a bulk-metallic glass. Appl. Phys. Lett. 86, 141904.
Yang, Q., Mota, A., Ortiz, M., 2006b. A finite-deformation constitutive model of bulk metallic glass plasticity. Comput. Mech. 37, 194–204.
Zener, C., Hollomon, J.H., 1944. Effect of strain rate upon plastic flow of steel. J. Appl. Phys. 15, 22–32.
Zhang, H.W., Subhash, G., Maiti, S., 2007. Local heating and viscosity drop during shear band evolution in bulk metallic glasses under quasistatic loading. J. Appl. Phys. 102, 043519.
Zhang, H.W., Maiti, S., Subhash, G., 2008. Evolution of shear bands in bulk metallic glasses under dynamic loading. J. Mech. Phys. Solids 56, 2171–2187.
Zhang, Y., Greer, A.L., 2006a. Thickness of shear bands in metallic glasses. Appl. Phys. Lett. 89, 071907.
Zhang, Y., Wang, W.H., Greer, A.L., 2006b. Making metallic glasses plastic by control of residual stress. Nat. Mater. 5, 857–860.
Zhang, Z., Clifton, R.J., 2003. Shear band propagation from a crack tip. J. Mech. Phys. Solids 51, 1903–1922.
Zhang, Z.F., Eckert, J., Schultz, L., 2003. Difference in compressive and tensile fracture mechanisms of $Zr_{59}Cu_{20}Al_{10}Ni_3Ti_3$ bulk metallic glass. Acta Mater. 51, 1167–1179.
Zhao, M., Li, M., 2008. Interpreting the change in shear band inclination angle in metallic glasses. Appl. Phys. Lett. 93, 241906.
Zhou, F., Wright, T.W., Ramesh, K.T., 2006. The formation of multiple adiabatic shear bands. J. Mech. Phys. Solids 54, 1376–1400.